Non-lagging effect of motorcycle tyres

Non-lagging effect of motorcycle tyres

An experimental study with the Flat Plank Tyre Tester

Author: R.T. Uil
Report No. DCT 2006.046

Internal traineeship

Supervisors:
Dr. Ir. A.J.C. Schmeitz
Dr. Ir. I.J.M. Besselink
Prof. Dr. H. Nijmeijer

Eindhoven University of Technology
Department of Mechanical Engineering
Dynamics and Control Technology Group

Eindhoven, June 2006

Summary

In this report the non-lagging effect of motorcycle tyres is studied experimentally. Important aspects in motorcycle behaviour are the large camber changes while cornering. When a non-rolling cambered wheel is vertically loaded against the road or when an upright tyre is loaded against a cambered road surface, it turns out that a side force is developed instantaneously. This is caused by the non-symmetric deformation of the cross section of the lower part of the tyre. If the tyre starts rolling, the side force will build up as a result of camber and/or side slip.

The aim of this report is to investigate the non-lagging lateral force and the development of the side force of motorcycle tyres during cambering of the tyre for different loading conditions. To achieve this objective several experiments have been performed with the Flat Plank Tyre Tester, including stiffness, relaxation and camber measurements. From the results, characteristics for the development of the forces and moments at the tyre contact centre and the non-lagging part fractions, to characterize the non-lagging tyre behaviour, are obtained.

From the measurement results it can be concluded that:

- The loading case of the tyre has the most influence on the contribution of the non-lagging side force, which is developed directly after the wheel is cambered.
- The vertical load is less important for the non-lagging tyre behaviour.
- The sign of the side force always acts in the same direction as the steady-state side force.

When a comparison is made between the measurements with a positive or a negative camber angle, it occurs that:

- The steady-state side force does not correspond for measurements with positive and negative camber angles.
- As a result, for measurements where an upright tyre is vertically loaded against a cambered track, non-lagging part fractions larger than 100 percent are obtained.

For further investigation of the non-lagging behaviour of motorcycle tyres, it is recommended that:

- More camber measurements have to be performed with several motorcycle tyres. Emphasize in this investigation should be laid on:
  - Different loading cases.
  - Differences between positive and negative camber angles
- Determine the necessary parameters to build the semi-empirical tyre model that is used to describe the non-lagging effect for car tyres.
- Validate if this existing tyre model (used for car tyres) also predicts the non-lagging tyre behaviour of motorcycle tyres.

Samenvatting

In dit verslag is de instantane responsie van een deel van de spoorkracht voor motorfietsbanden experimenteel onderzocht. Een belangrijk aspect in het gedrag van motorfietsen is de grote wielvluchtveranderingen bij het rijden in een bocht. Wanneer een stilstaande band onder wielvlucht verticaal wordt belast of een rechtopstaande band verticaal tegen een wegdek onder wielvlucht wordt belast, dan zal er onmiddellijk een spoorkracht ontwikkeld worden. Wanneer de band begint te rollen, dan zal de spoorkracht toenemen als een gevolg van wielvlucht en/of dwarsslip.

Het doel van dit verslag is het onderzoeken van de instantane responsie van een deel van de spoorkracht en de ontwikkeling van de spoorkracht van motorfietsbanden bij het rijden door een bocht. Dit gedrag is onderzocht voor verschillende manieren van aanbrengen van de normaalbelasting. Om deze doelstellingen te bereiken, zijn verschillende experimenten op de bandentestbank uitgevoerd. De uitgevoerde experimenten bestonden uit stijfheids-, relaxatie- en wielvluchtmetingen. Uit de resultaten zijn verschillende karakteristieken voor de krachten en momenten in het bandcontactvlak en de fractie die het responsiegedrag van de spoorkracht karakteriseert bepaald

Uit de resultaten kan het volgende geconcludeerd worden:

- De manier van aanbrengen van de normaalbelasting heeft de meeste invloed op de bijdrage van de instantane responsie van een deel van de spoorkracht.
- De verticale belasting heeft veel minder invloed op het bandgedrag bij het aanbrengen van wielvlucht op de motorfietsband.
- De richting van de spoorkracht werkt altijd in dezelfde richting als de te bereiken stationaire spoorkracht.

Uit de vergelijking tussen metingen met positieve en negatieve wielvluchthoeken, kan het volgende geconcludeerd worden:

- Er treedt een verschil op in de ontwikkelde stationaire spoorkracht voor positieve en negatieve wielvluchthoeken.
- Met als gevolg dat bij de metingen waar een rechtopstaande band verticaal tegen een wegdek onder een wielvluchthoek wordt belast, er fracties van het responsiegedrag van de spoorkracht groter dan 100 procent optreden.

Voor het verder onderzoeken van het bandgedrag van motorfietsbanden bij het rijden in bocht, zijn de volgende aanbevelingen gemaakt:

- Voor het onderzoeken van het bandgedrag en de instantane responsie die optreedt bij het aanbrengen van wielvlucht, is het aan te bevelen om meer metingen met verschillende typen motorfietsbanden te verrichten. De nadruk tijdens deze metingen zou moeten liggen op:
  - De verschillende manieren van aanbrengen van de normaalbelasting, omdat is gebleken dat dit de meeste invloed heeft op de responsie die optreedt bij wielvlucht.
  - De verschillen tussen de resultaten van positieve en negatieve wielvluchthoeken moeten verder onderzocht worden.
- Bepaal de benodigde parameters voor het bouwen van het semi-empirisch band model, dat is gebruikt om de responsie van een deel van de spoorkracht als gevolg van wielvlucht voor normale autobanden te beschrijven.
- Valideer of het bestaande bandmodel (dat gebruikt wordt voor autobanden) de responsie van een deel van de spoorkracht ook voor motorbanden goed beschrijft.

Table of Contents

Summary ii
Samenvatting iii
List of Symbols v
1 Introduction 1
1.1 Motivation and background 1
1.2 Aim and scope 2
1.3 Contents of this report 2
2 Description of the measuring conditions 3
2.1 Flat Plank Tyre Tester 3
2.2 Measuring hub 3
2.3 Transformation of the forces and moments 4
3 Explanation of the performed measurements 8
3.1 Measurement conditions 8
3.2 Unloaded and loaded tyre radius 9
3.3 Vertical and lateral stiffness experiments 10
3.4 Relaxation measurements 13
3.5 Camber measurements 15
3.5.1 Measurement 37Z 15
3.5.2 Measurement 38R 15
3.5.3 Measurement 38C 16
3.6 Data processing 16
4 Discussion of the results of the camber measurements 17
4.1 Results non-lagging effect 17
4.2 Discussion of the results between the old and new tyre 20
5 Conclusions and recommendations 23
References 25
Appendix I 26
Derivation of the right-handed axis system in the tyre contact centre 26
Appendix II 28
Calibration LVDT 28
Appendix III 29
Slip angle measurement for checking lateral force at measuring hub 29
Appendix IV 30
Description measurement files 30
Appendix V 31
Overview of the performed measurements in this study 31

List of Symbols

C_{Fy}	[N/m]	lateral stiffness
$C_{F\alpha}$	[N/deg]	cornering stiffness
C_{Fz}	[N/m]	vertical stiffness
$\underline{\vec{e}}^{a}$	[-]	axle axis system
$\underline{\vec{e}}^{w}$	[-]	wheel axis system
F_x	[N]	longitudinal force (of the tyre)
F_y	[N]	side force (of the tyre)
$F_{y,NL}$	[N]	non-lagging lateral force (of the tyre)
$F_{y,ss}$	[N]	steady-state side force (of the tyre)
F_z	[N]	vertical force (of the tyre)
k	[-]	amplification ratio LVDT
K_x	[N]	longitudinal force (of the measuring hub)
K_y	[N]	side force (of the measuring hub)
K_z	[N]	vertical force (of the measuring hub)
M_x	[Nm]	overturning moment (of the tyre)
M_y	[Nm]	rolling resistance moment (of the tyre)
M_z	[Nm]	aligning torque (of the tyre)
T_x	[Nm]	moment about the x-axis (of the measuring hub)
T_y	[Nm]	moment about the y-axis (of the measuring hub)
T_z	[Nm]	moment about the z-axis (of the measuring hub)
r_0	[m]	free unloaded radius
r_e	[m]	effective rolling radius
r_l	[m]	loaded tyre radius
t_p	[m]	pneumatic trail
α	[rad]	slip angle
ε_{NL}	[-]	non-lagging part ratio
γ	[rad]	camber angle
ρ_{z0}	[m]	radial tyre deflection
ρ_y	[m]	lateral tyre deflection
ρ_z	[m]	vertical tyre deflection
σ_α	[m]	relaxation length with respect to side slip
ω	[m]	circumference of the tyre
Ω	[rad/s]	angular velocity

1 Introduction

1.1 Motivation and background

This report is the result of the work done for my internal training period. Currently in the Dynamics and Control Group several projects are carried out to develop a dynamic tyre model for motorcycle tyres. An important aspect in motorcycle behaviour are the large camber changes while cornering. During these camber changes a non-lagging side force occurs as a result of the asymmetric deformation of the tyre carcass. The main topic of this internal traineeship is to investigate the non-lagging tyre behaviour of motorcycle tyres. For normal car tyres this behaviour is already extensively investigated by Pacejka and Higuchi. It is also implemented in a semi-empirical tyre model for car tyres to simulate the development of the non-lagging lateral force. It is unknown if this behaviour develops the same for motorcycle tyres and if it is possible to use the same tyre model to simulate the non-lagging behaviour, because there is not many information available of the behaviour of motorcycle tyres.

Non-lagging effect:
When a non-rolling cambered wheel is vertically loaded against the road or when an upright tyre is loaded against a cambered road surface, it turns out that a side force is developed instantaneously. This is caused by the non-symmetric deformation of the cross section of the lower part of the tyre. The side force that arises is called the non-lagging lateral force (Pacejka, 2002). When the tyre starts rolling, the lateral force starts to build up from this non-lagging force level to its final steady-state value. The amount of non-lagging lateral force that arises is difficult to predict, because it depends on the way the tyre is loaded (Schmeitz, 2004).
To investigate the amount of non-lagging lateral force, several experiments have been performed for different loading conditions.

To characterize the non-lagging lateral force, the non-lagging part fraction (ε_{NL}) is proposed by Pacejka (Pacejka, 2002) and Higuchi (Higuchi, 1997a). This fraction is defined as:

$$\varepsilon_{NL} = \frac{F_{y,NL}}{F_{y,SS}} \tag{1.1}$$

In this equation $F_{y,NL}$ and $F_{y,SS}$ are the non-lagging lateral force and steady-state lateral force, respectively. This fraction depends on the loading condition, the applied vertical load and the applied camber angle. In this project experiments have been performed for three different loading conditions and for several camber angles.

The force response to a change in camber is already investigated for car tyres and described by Pacejka. Low velocity experiments have been conducted on the Flat Plank Tyre Tester. Figure 1.1 gives the percentage of the non-lagging part with respect to the steady-state side force for three wheel loads and for three different ways of reaching the loaded and cambered condition before rolling has started (Pacejka, 2002).
In the results three different appellations have been used for the loading conditions. Case Z represents the loading case where the tyre is first cambered and than vertically loaded against the track. For case R the track is first cambered and after that the tyre is vertically loaded against the track. In the last case, case C, the tyre is first vertically loaded against the

track and after loading the track of the Flat Plank Tyre Tester is cambered. In figure 1.1 these three different loading cases are depicted.

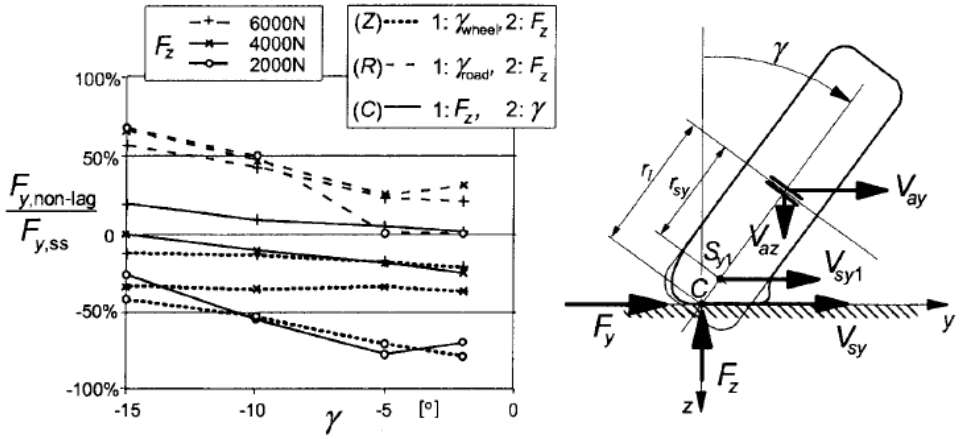

Fig. 1.1 Results of the non-lagging part of side force response for car tyres.

The loading sequence (Z) appears to result in a somewhat larger non-lagging part. For loading sequence (R) it turns out that the response arises with the same sign as the steady-state response. The diagram indicates that also in case (C) the sign may remain unchanged if the wheel load is sufficiently high (Pacejka, 2002).

1.2 Aim and scope

The objective of this internal traineeship is to investigate the non-lagging effect for motorcycle tyres. Emphasize will be laid on the determination of the non-lagging part and the build up of the lateral force to the steady-state value for different loading conditions. Another important part is to determine all the measurement data necessary to calculate the parameters with which a semi-empirical tyre model can be developed to simulate the development of the non-lagging lateral force.
The aim of this internal traineeship is:
Investigate the non-lagging lateral force and the development of the steady-state side force for different loading conditions.

To achieve this objective several experiments have been performed on the Flat Plank Tyre Tester, including slip angle, camber, stiffness and relaxation measurements. Out of the results characteristics for the development of the forces and moments at the tyre contact centre are obtained. Also characteristics for the vertical and lateral stiffness are obtained to give an indication of the nonlinear behaviour of the motorcycle tyre. From these results the non-lagging part fraction for motorcycle tyres is obtained, to characterize the non-lagging tyre behaviour during cornering.

1.3 Contents of this report

Chapter 2 consists of a description of the measuring conditions, which are applicable for the measurements performed with the Flat Plank Tyre Tester. After that, in chapter 3 an explanation of the performed measurements to investigate the motorcycle tyre behaviour is given. The results will be discussed in chapter 4, where emphasize is laid on the non-lagging effect for motorcycle tyres. Also, a comparison between measurements with a new and old tyre is described in this chapter. The last chapter gives the conclusions and recommendations of this research. Finally, in the appendix a complete overview of the test results and the description of the measurement files, which are included on a CD-Rom, are given.

2 Description of the measuring conditions

2.1 Flat Plank Tyre Tester

For all the measurements performed during this training period the Flat Plank Tyre Tester is used. In figure 2.1 an illustration of the Flat Plank Tyre Tester is depicted.

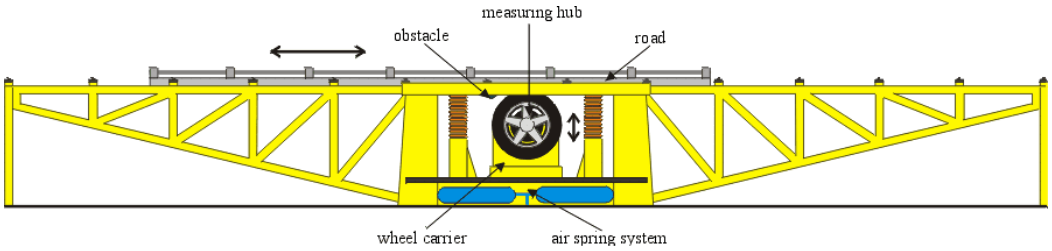

Fig. 2.1 Flat Plank Tyre Tester

The road surface is upside-down on top of the machine and it can move with a maximum speed of 4.75 cm/s. Under the road a measuring hub is placed on which it is possible to mount a tyre. The measuring hub measures the forces and moments at the wheel axle. Two different methods are available to vertically load the tyre. The first method is to adjust the axle height by a jack to vary the vertical load; the axle height will stay constant during the measurement. The second method is to apply the vertical load with the aid of the air spring system. The vertical load is adjusted by changing the pressure in the air spring system. With this system the vertical load will stay almost constant during the measurement and therefore it is very suitable for measurements while driving over an obstacle (cleat measurement). For the camber measurements, the vertical load is always applied using the first method (constant axle height).

Another possible movement of the measuring hub is the rotation around the vertical axis of the turn table. This movement is suitable to measure for example with a side slip angle. In this research it is used to perform the relaxation measurements.
For the adjustment of the inclination angle of the Flat Plank Tyre Tester, two methods are available. The first method is to apply a hydraulic pressure on the measuring hub, after that it is possible to adjust the angle of the hub. With the second method it is possible to adjust the inclination angle of the track with an actuator. Both methods are used to perform camber measurements with the motorcycle tyre.

The forces and moments at the wheel axle are measured with strain gauge bridges. These measured signals are amplified and low pass filtered, before they are converted into a digital signal and sampled in the measurement PC.

2.2 Measuring hub

As mentioned above the forces and moments are measured at the wheel axle with the measuring hub. In figure 2.2 a detailed overview of the measuring hub is given. In the left figure the five strain gauge bridges of the measuring hub are depicted. The voltages measured with these strain gauge bridges are used to calculate the forces and moments at the measuring hub depicted in the right figure. The following forces and moments are measured: longitudinal force K_x, lateral force K_y, vertical force K_z, moment about the x-axis T_x and moment about the z-axis T_z. The moment about the y-axis T_y is zero, because

the wheel is not driven or braked and consequently the wheel is freely rolling during the measurements.

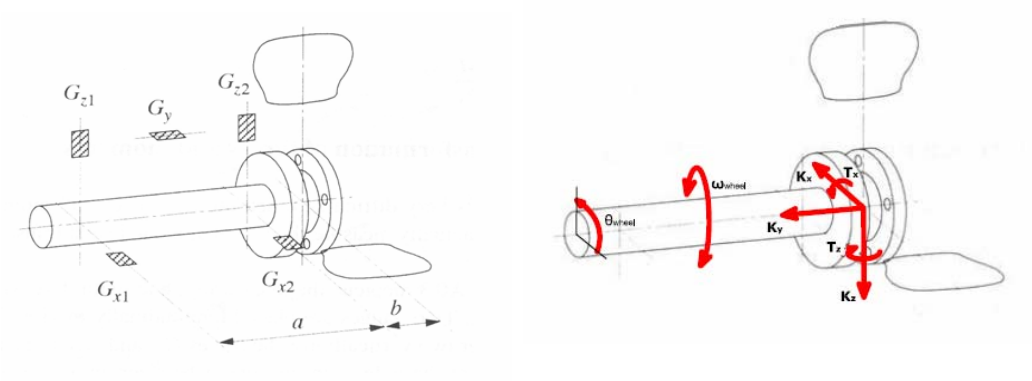

Fig. 2.2 Overview forces and moments in the measuring hub

The resulting forces and moments are:

$$
\begin{aligned}
K_x &= G_{x1} + G_{x2} \\
K_y &= G_y \\
K_z &= G_{z1} + G_{z2} \\
T_x &= G_{z1}(a+b) + G_{z2}b \\
T_y &= 0 \\
T_z &= G_{x1}(a+b) + G_{x2}b
\end{aligned}
\qquad (2.1)
$$

2.3 Transformation of the forces and moments

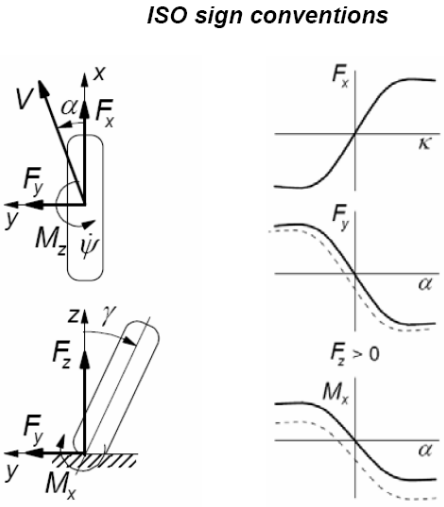

For the investigation of the tyre behaviour, the forces and moments working at the tyre contact patch are necessary. Because the coordinate system of the measuring hub is not a right-handed coordinate system, the coordinate axis system has to be transformed into a right-handed coordinate system in the contact patch.

All the forces and moments that will be introduced hereafter are conform the ISO-definitions, which means that the coordinate system is right-handed and the z-axis is perpendicular to and points away from the road surface; the x-axis is parallel to the road surface and point in the driving direction. The ISO sign conventions are depicted on the left in figure 2.3.

Fig. 2.3 ISO sign conventions

In appendix I a derivation of the forces and moments for a rotation about the x-axis, which corresponds with a camber angle, is described. The outcome of this derivation is used to calculate the forces and moments at the tyre contact centre. The forces indicated with F and moments with M are the forces and moments at the tyre contact centre and those which are indicated with K and T are the forces and moments in the measuring hub. Below the relations are given for right-handed axis systems:

$$\begin{bmatrix} F_x \\ F_y \\ F_z \end{bmatrix} = \begin{bmatrix} K_x^* \\ K_y^* \cos(\gamma) - K_z^* \sin(\gamma) \\ K_y^* \sin(\gamma) + K_z^* \cos(\gamma) \end{bmatrix}$$
$$\begin{bmatrix} M_x \\ M_y \\ M_z \end{bmatrix} = \begin{bmatrix} T_x^* - r_l K_y^* \\ T_y^* \cos(\gamma) - T_z^* \sin(\gamma) + K_x^* r_l \cos(\gamma) \\ T_y^* \sin(\gamma) + T_z^* \cos(\gamma) + K_x^* r_l \sin(\gamma) \end{bmatrix} \qquad (2.2)$$

The stars (*) are used to indicate that the forces and moments are defined with respect to a right-handed axis system. In the next section a derivation of the forces and moments at the contact centre is given for both directions of travel of the Flat Plank Tyre Tester.

First situation:

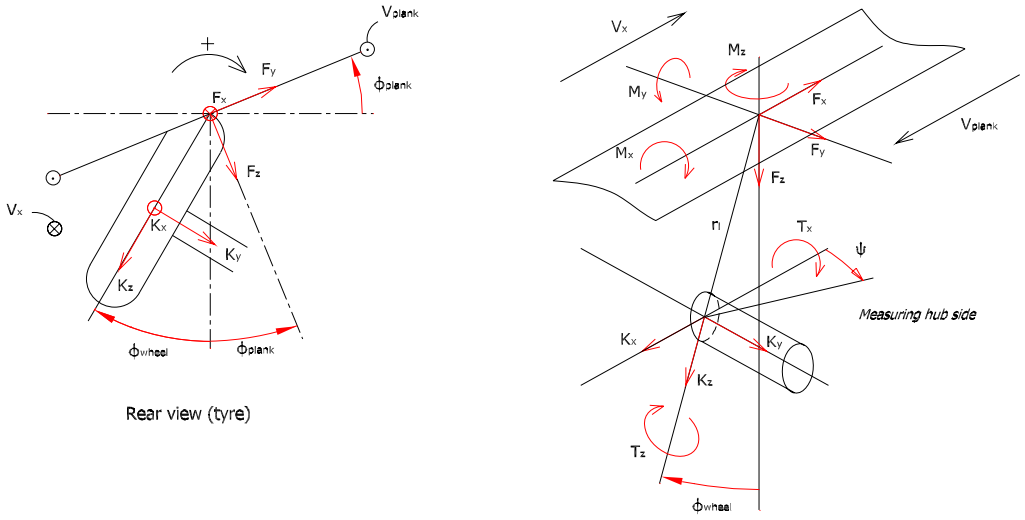

Fig. 2.4 Overview forces and moments for the first movement direction

In figure 2.4 the coordinate system of the measuring hub at the contact centre is depicted. The direction of travel of the road V_{plank} (V_{plank}) is to the left, which is shown in the right figure. In the left figure the situation is depicted when the tyre or the road is cambered with a positive angle. For this direction of travel and camber angle, the forces and moments have been derived.
The following variables have been defined to transform the coordinate system of the measuring hub into a right-handed axis system. The forces and moments indicated with a star (*) are the variables in the right-handed axis system. With this transformation it is easier to derive the equations of motion at the contact centre.

$$\begin{aligned} K_x^* &= -1 \cdot K_x & T_x^* &= T_x \\ K_y^* &= K_y & T_y^* &= 0 \\ K_z^* &= K_z & T_z^* &= T_z \end{aligned} \tag{2.3}$$

To get the set of equations for this situation, the variables defined in (2.3) have to be substituted in equations (2.2). This results in the following set of equations:

$$\begin{aligned} F_x &= -K_x \\ F_y &= K_y \cos\gamma - K_z \sin\gamma \\ F_y &= K_y \sin\gamma + K_z \cos\gamma \\ M_x &= T_x - r_l K_y \\ M_y &= -T_z \sin\gamma - r_l K_x \cos\gamma \\ M_z &= T_z \cos\gamma - r_l K_x \sin\gamma \end{aligned} \tag{2.4}$$

In these equations r_l is the loaded radius, thus a positive value.
Further, note that the camber angle γ is defined as:

$$\gamma = \phi_{wheel} - \phi_{plank} \tag{2.5}$$

Note that in figure 2.4 ϕ_{plank} has a negative sign.

Second situation:
In the second situation the direction of travel of the road is in the opposite direction. In this situation V_{plank} is to the right as depicted in de right figure. Because of this opposite direction, the direction for a positive camber angle has changed. The direction of the forces and moments has also changed and therefore different equations are applicable in the contact centre. Therefore the following variables indicated with a $(*)$ have been defined to transform the coordinate system at the wheel axle into a right-handed axis system. Again, the variables with a $(*)$ are in the right-handed axis system.

$$\begin{aligned} K_x^* &= K_x & T_x^* &= -1 \cdot T_x \\ K_y^* &= -1 \cdot K_y & T_y^* &= 0 \\ K_z^* &= K_z & T_z^* &= T_z \end{aligned} \tag{2.6}$$

By solving the same set of equations as in (2.2), the following equations are obtained:

$$\begin{aligned} F_x &= K_x \\ F_y &= -K_y \cos\gamma - K_z \sin\gamma \\ F_z &= -K_y \sin\gamma + K_z \cos\gamma \\ M_x &= -T_x + r_l K_y \\ M_y &= -T_z \sin\gamma + r_l K_x \cos\gamma \\ M_z &= T_z \cos\gamma + r_l K_x \sin\gamma \end{aligned} \tag{2.7}$$

Note that:

$\gamma = \phi_{wheel} - \phi_{plank}$, as defined in equation (2.5).

And that ϕ has the same sign as γ, thus positive anti-clockwise in the left figure of figure 2.5.

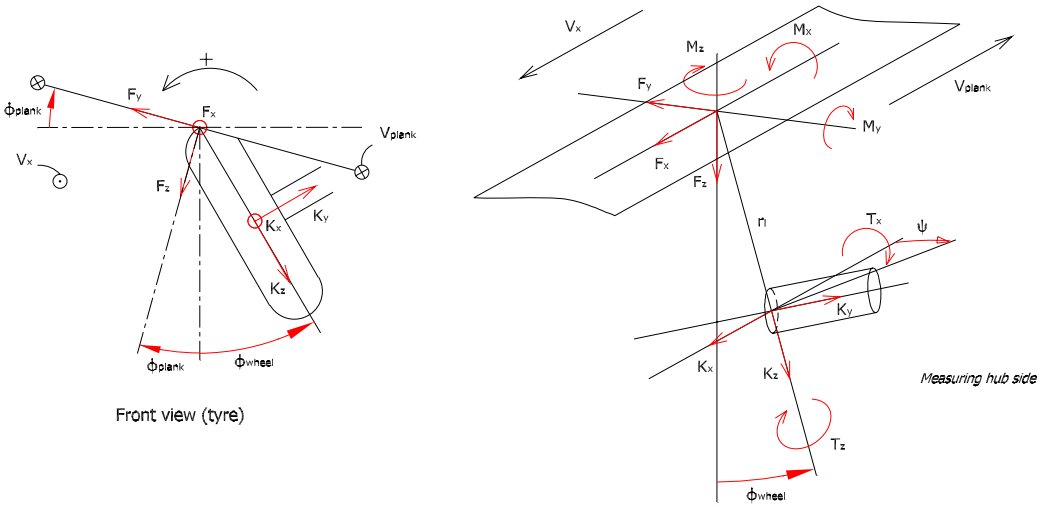

Fig. 2.5 Overview forces and moments for the second situation

3 Explanation of the performed measurements

For the research of the non-lagging effect for motorcycle tyres, several experiments have been performed to acquire a lot of information of the tyre behaviour for motorcycle tyres. Not only camber measurements are performed, but also stiffness and relaxation experiments. In this chapter the measurement conditions and the experiments as well as the data processing will be discussed.

3.1 Measurement conditions

All the measurements for the research are performed with the motorcycle tyre:

Dunlop Sportmax D220-ST
200/50ZR17

For all measurements, the inflation pressure is kept constant at 2.5 bar. Because the motorcycle tyre has one direction of rotation, the experiments are only performed in that direction. For the processing of the measurement data, the equations of (2.4) are used in this situation, because they correspond with the right direction of rotation of the tyre.

For the camber measurements the variations in vertical load and camber angle are used:

$$F_z = 1400, 1950, 2500\,\mathrm{N}$$
$$\gamma = -15 \ldots 15\,\mathrm{deg}$$

To compensate for tyre non-uniformities, the measurements are started from three different positions on the tyre (markers are placed on the tyre at 120 degrees difference from each other). From the three date files of a measurement the average is calculated to collect the final data for that measurement.

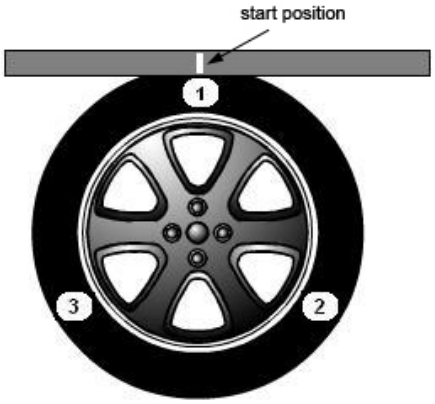

In figure 3.1 an example is presented of the three markers on the tyre. These markers represent the three starting positions for every measurement. The starting position on the track is indicated through a trigger unit and the sampling starts by a triggering signal. The measurement data that is collected during a measurement is always measured at the same section on the track. To minimize the dead band until the sampling starts, the initial longitudinal gap in the trigger unit should be set as small as possible.

Fig. 3.1 Starting positions measurements

When tyres are rolling with zero camber and zero slip angle, they usually produce a non-zero side force and aligning torque. This phenomenon is due to the effects of plysteer and conicity. Plysteer is caused by the effect of the construction and build-up of the carcass layers. Conicity is caused by the shape of the tyre/carcass (production tolerances).

To investigate the non-lagging effect of motorcycle tyres, it is not desired to see these effects in the measurement results. Therefore, before the start of a measurement a reference measurement will be carried out to eliminate these effects. Figure 3.2 shows an example of the data correction of the side force and aligning torque respectively.

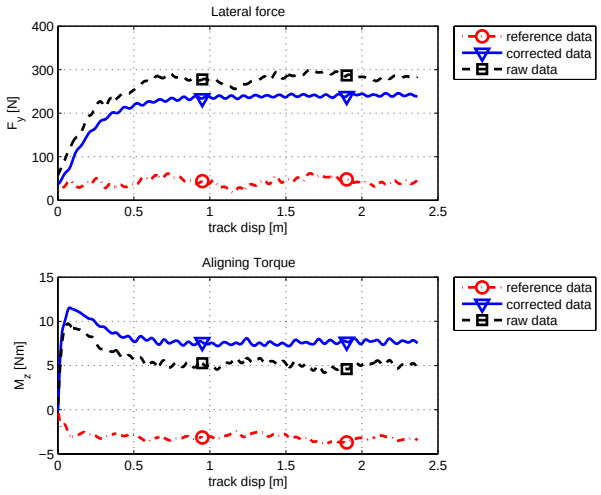

Fig. 3.2 Example of data correction: F_z = 1950 N, γ = -5°

The reference measurements are performed at zero slip angle and zero camber angle. The corrected data is obtained by subtracting the reference data from the raw data. This process is applied to the longitudinal force F_x, the side force F_y, the overturning moment M_x and the aligning torque M_z. To get accurate results for every measurement, it is important that the markers on the tyre and the track coincide with each other each time before the measurement is started.

A complete overview of all the measurement results is enclosed in Appendix V. In the following paragraphs the performed experiments and the data processing will be discussed.

3.2 Unloaded and loaded tyre radius

The unloaded radius r_0 of the tyre is measured with the aid of a rope to measure the circumference ω of the tyre:

$$r_0 = \frac{\omega}{2\pi} = 318.3\,\text{mm} \tag{3.1}$$

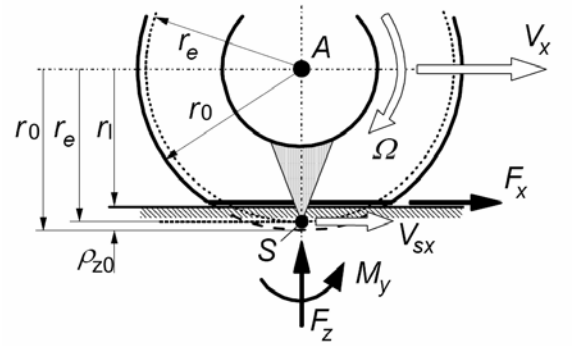

Fig. 3.3 Overview different tyre radii

To determine the loaded tyre radius r_l for the different loading conditions, the vertical tyre deflection ρ_{z0} at the specific vertical load is needed.

The loaded tyre radius is defined as:

$$r_l = r_0 - \rho_{z0} \tag{3.2}$$

The vertical tyre deflection is determined with experiments on the Flat Plank Tyre Tester. The tyre is vertically loaded against the track until the desired vertical load is reached. The measurement is started and the measured vertical tyre deflection is determined with the LVDT.

The results are:

F_z [N]	ρ_{zo} [m]	r_l [m]
1400	0.007913	0.3078
1950	0.01077	0.3051
2500	0.01370	0.3021

Table 3.1 Results loaded tyre radius

Subsequently, the loaded tyre radius is used in calculation of the moments at the tyre contact centre.

3.3 Vertical and lateral stiffness experiments

The vertical C_{Fz} and lateral C_{Fy} stiffness are important tyre parameters for tyre modelling. Therefore measurements have been performed to determine these parameters, so that for further investigation in the behaviour of motorcycle tyres these parameters are known.

Vertical stiffness experiment:
The vertical tyre force vs. vertical deflection is an important tyre characteristic:

- The vertical tyre stiffness influences the natural frequencies of the vibrations of the tyre (Zegelaar, 1998).
- The tyre is excited by road unevenness through the vertical tyre stiffness (Zegelaar, 1998).

The vertical stiffness gives an interpretation of the relation between the applied vertical load and the vertical tyre deflection. In general it is defined as the following ratio.

$$C_{Fz} = \frac{\partial F_z}{\partial \rho_z} \tag{3.3}$$

The vertical stiffness experiment is carried out to proportionally build up the vertical load to a final value of 3000 N and then decrease the vertical load to zero. In the measurement this action is repeated three times, to get a good result for the entire tyre. The measured vertical force is fitted with a second order polynomial as function of the vertical deflection. Subsequently, the vertical tyre stiffness is obtained from differentiating the polynomials with respect to the vertical tyre deflection at different levels of the vertical load. These experiments have been performed with a rolling tyre and also with a non-rolling tyre, to determine if there is any difference between both methods. In figure 3.4 an overview of the results is depicted.

From figure 3.4a all the data above F_z=10[N] is selected and shifted along the horizontal axis to zero. The selected data (figure 3.4b) can be described with the following second order polynomial fit:

$$F_z = 1.9529\rho_z^2 + 115.36\rho_z \tag{3.4}$$

The vertical stiffness can be determined using the following equation:

$$C_{Fz} = \frac{\partial F_z}{\partial \rho_z} = 3.9058\rho_z + 115.36 \tag{3.5}$$

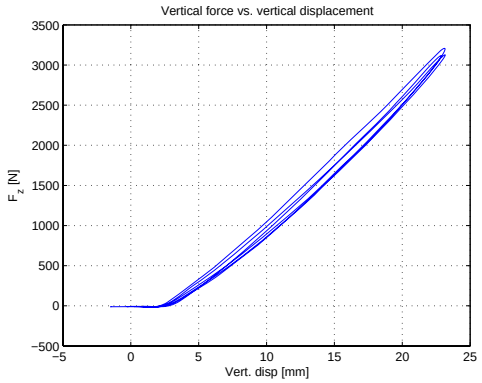

Fig. 3.4a raw data

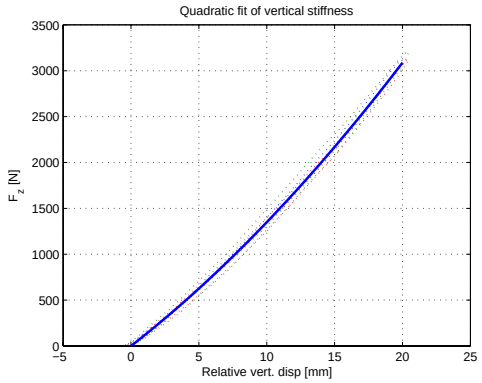

Fig. 3.4b selected data + fit

Using equation(3.5), the nonlinear vertical stiffness is determined.

F_z [N]	ρ_z [mm]	C_{Fz} [N/m]
1400	10.33	155700
1950	13.72	168950
2500	16.86	181200

Table 3.2 Results vertical stiffness for a rolling tyre

For the non-rolling tyre the same experiment is performed. The only difference with the rolling experiment is that in this case the track of the Flat Plank Tyre Tester does not move when the tyre is vertically loaded. The results are depicted in figure 3.5.

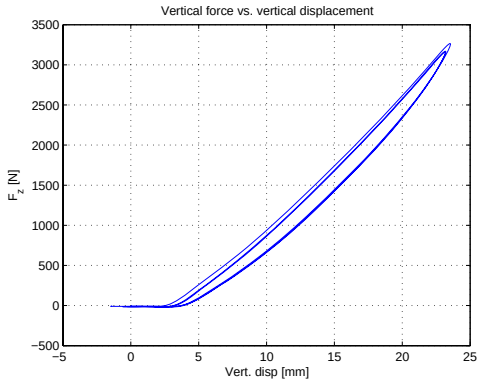

Fig. 3.5a raw data

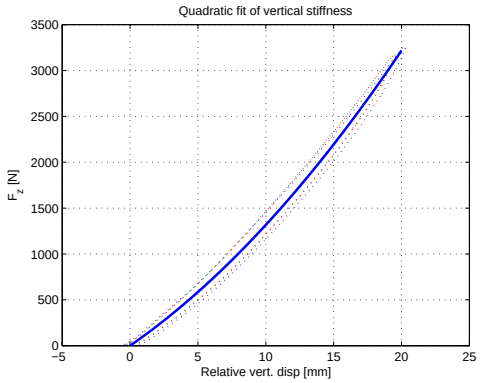

Fig. 3.5b data selected + fit

The resulting second order polynomial fit, describing the data selection in figure 3.5b is:

$$F_z = 2.9205\rho_z^2 + 102.5\rho_z \tag{3.6}$$

The vertical stiffness can be determined using the following equation:

$$C_{Fz} = \frac{\partial F_z}{\partial \rho_z} = 5.8410\rho_z + 102.5 \tag{3.7}$$

The nonlinear vertical stiffness for the non-rolling tyre is.

F_z [N]	ρ_z [mm]	C_{Fz} [N/m]
1400	10.51	163900
1950	13.69	182500
2500	16.57	199300

Table 3.3 Results vertical stiffness for the non-rolling tyre

Between both measurement methods different results for the magnitude of the vertical stiffness for different vertical loading conditions occurs. The vertical stiffness for the non-rolling tyre is slightly higher than for the rolling tyre. The results also indicate that the vertical stiffness of the motorcycle tyre shows a nonlinear behaviour.

This phenomenon is also studied for normal car tyres in the PhD Thesis of Zegelaar (Zegelaar, 1998). The static stiffness of a non-rotating tyre is measured on both the 2.5 m drum and the flat road. The Dynamic stiffness of both a non-rotating and a rotating tyre have been obtained from small amplitudes of random axle height vibrations around four average vertical loads. In the second method, the dynamic stiffness is obtained from large sinusoidal axle height motions. The dynamic stiffness experiments are measured on the 2.5 m drum. From these experiments it can be concluded that the measured dynamic vertical tyre stiffness is somewhat lower than the static vertical tyre stiffness measured on a flat road. The static vertical stiffness measured on the 2.5 m drum is lower than the stiffness on the road, caused by the influence of the drum radius.
In conclusion, the same behaviour of the vertical stiffness for motorcycle tyres is obtained as for car tyres when the vertical stiffness is measured on a flat road.

Lateral stiffness experiment:
The lateral stiffness is defined as the derivative of the lateral force F_y versus the lateral tyre deflection ρ_y. Here, the lateral stiffness C_{Fy} represents the slope of the linear section of the lateral force versus the lateral deflection:

$$C_{Fy} = \left.\frac{\partial F_y}{\partial \rho_y}\right|_{\rho y=0} \tag{3.8}$$

For this measurement it is necessary to rotate the measuring hub 90 degrees, so the tyre is placed perpendicular to the driving direction. So the tyre is pulled over the track and is consequently not rolling. The total measuring time for this experiment is very short, because the tyre will reach its maximum lateral force soon and than stick slip occurs. At this point the lateral force does not further increase. Over the range where the lateral force builds up, it is possible to determine the lateral stiffness.

In figure 3.6 the results of the measurement at three different vertical loads are shown.

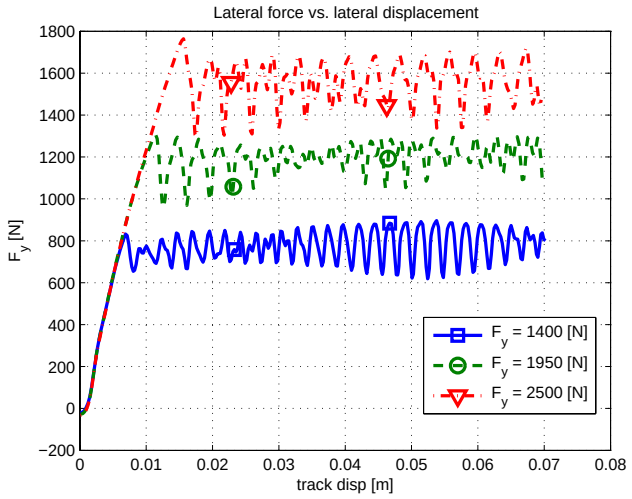

Fig. 3.6 Lateral stiffness results

For the different vertical loads, the lateral stiffness is determined by calculating the stiffness using the linear section of the results shown in figure 3.6. Since, the lateral stiffness values are very similar, the final value for the lateral stiffness of the motorcycle tyre is determined from the mean of the three calculated lateral stiffnesses.

F_z [N]	F_y [N]	d_y [mm]	C_{Fy} [N/m]
1400	724	5.703	126950
1950	1170	9.410	124350
2500	1512	12.630	119700

Table 3.4 Results lateral stiffness

This gives the final value for the lateral stiffness:

$$C_{F_y} = 123700[N/m]$$

3.4 Relaxation measurements

Steady-state tyre models will lose their validity when the motion of the wheel shows variations in time as the horizontal tyre deformation does not instantaneously follow slip variations. To build up a horizontal deflection the tyre has to travel a certain distance. The distance travelled needed to reach 63% of the steady-state deflection after a step change is generally designated as relaxation length and is approximately independent of the running speed of the tyre (Zegelaar, 1998).

To investigate the relaxation behaviour of the motorcycle tyre, an experiment has been performed to determine the response of the tyre to a slip angle change of one degree. This experiment is performed for the three different vertical loads and in figure 3.7 the results are depicted. The reference measurement at zero degrees is subtracted from the data measured at one degree slip angle.

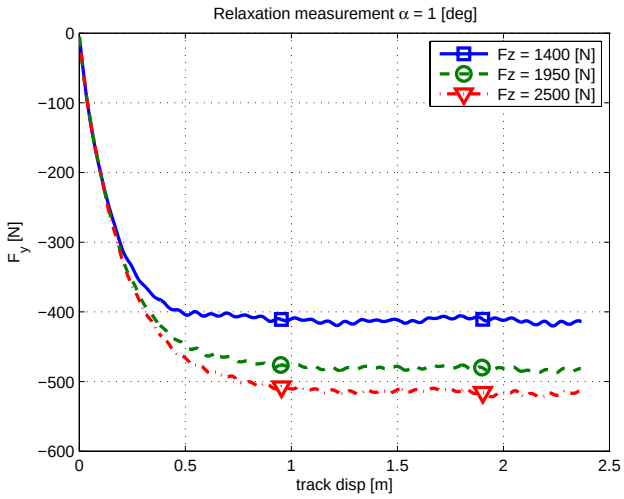

Fig. 3.7 Results relaxation measurement

From the results an approximation of the cornering stiffness is determined as:

$$C_{F\alpha} \approx \frac{F_{y,ss}}{\alpha} \tag{3.9}$$

It can be concluded that the cornering stiffness increases for an increasing vertical load. For the vertical loading conditions, the following cornering stiffnesses are determined:

F_z [N]	$F_{y,ss}$ [N]	$C_{F\alpha}$ [N/deg]
1400	-410	410
1950	-480	480
2500	-513	513

Table 3.5 Result cornering stiffness

In (Pacejka, 2002) the relaxation length for side slip is defined as:

$$\sigma_{\alpha,pacejka} = \frac{C_{F\alpha}}{C_{Fy}} \tag{3.10}$$

Subsequently, the relaxation lengths are determined from the steady-state values of the lateral force and with the relation defined by Pacejka.

F_z [N]	σ_α [m]	$\sigma_{\alpha,pacejka}$ [m]
1400	0.150	0.185
1950	0.184	0.221
2500	0.200	0.246

Table 3.6 Relaxation lengths

For the relaxation behaviour of motorcycle tyres, it can be concluded that the relaxation length for side slip defined by Pacejka is higher than the relaxation length determined from the steady-state side force.

3.5 Camber measurements

The main topic of this internal training period is the investigation of the tyre behaviour of a motorcycle tyre during cambering. Several experiments have been performed to investigate the steady-state tyre behaviour. The development of forces and moments will differ if the process towards the final situation is different (Higuchi, 1997a). This development behaviour is investigated for three different loading processes, which will be discussed in the next section. The measurements are qualified as three different measurement numbers, which will also be used in the discussion of the results.

3.5.1 Measurement 37Z

Experiment procedure:

1. The track is placed horizontal.
2. Unloaded tyre is cambered to an inclination angle of γ = 2, 5, 10 or 15 degrees, so the inclination angle is applied to the measuring hub.
3. Next the tyre will be loaded vertically with F_z = 1400, 1950 or 2500 N.
4. Start the measurement.
5. Move the track.

Figure 3.8 shows a graphical representation of the loading process.

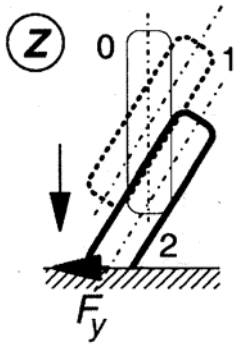

Fig. 3.8 Experiment procedure for measurement 37Z

3.5.2 Measurement 38R

Experiment procedure:

1. Initially unloaded tyre.
2. The track is turned to an inclination angle of γ = 2, 5, 10 or 15 degrees.
3. Next the tyre will be loaded vertically with F_z = 1400, 1950 or 2500 N.
4. Start the measurement.
5. Move the track.

In figure 3.9 a graphical representation of the loading process is presented.

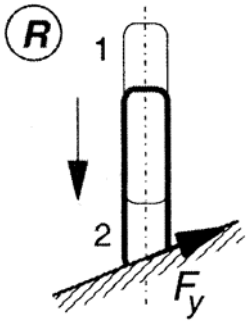

Fig. 3.9 Experiment procedure for measurement 38R

3.5.3 Measurement 38C

Experiment procedure:

1. Initially the track is placed horizontally and the wheel axle is horizontal as well. The wheel centre plane is going exactly through the axis of rotation of the road surface plane.
2. The tyre is vertically loaded against the track with F_z = 1400, 1950 or 2500 [N].
3. Next the track is cambered to an inclination angle of γ = 2, 5, 10 or 15 degrees.
4. Start the measurement.
5. Move the track.

In figure 3.10 a graphical representation of the loading process is presented.

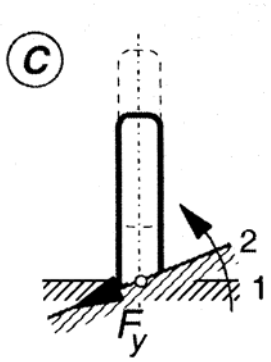

Fig. 3.10 Experiment procedure for measurement 38C

3.6 Data processing

The signals from the strain gauge bridges are sent to the strain gauge amplifier and sampled after A/D conversion by the data acquisition program in the personal computer and then stored on the hard disk. Subsequently the measuring data are transformed to data which are necessary for the investigation of the tyre behaviour. The data processing is performed by using Matlab. In the next overview, a short explanation of the data processing for a camber measurement is given:

- First, both the raw data file and the corresponding reference file are read into Matlab.
- Then, the reference data is subtracted from the data file for the signals: F_x, F_y, M_x and M_z.
- For the three vertical loads the loaded radius is calculated.
- Then the positive or negative camber angle is converted from degrees to radians.
- With the above parameters the forces and moments at the contact patch are calculated with the equations of (2.4).
- The converted data is placed in a new data matrix and from the three tyre measuring positions the average of the three data matrices is calculated.
- Subsequently the final data matrix is filtered using a 4^{th} order Butterworth low-pass filter with a cut-off frequency of 1 Hz.
- The filtered data is the final data, which is used to produce the several plots of the measurement results, shown in Chapter 4.

All the necessary data files which are used for processing the measurement data are included on a CD-Rom. The used unique filenames are explained in Appendix IV.

4 Discussion of the results of the camber measurements

In this chapter the results of the camber measurements as described in paragraph 3.5 will be discussed. Emphasize in the discussion of the results will be laid on the comparison between the different measurements and the changes in tyre behaviour caused by the variation in camber angle. During the measurements it appeared that a difference occurs between measuring with a positive and a negative camber angle. At the start of the measurements the motorcycle tyre, which was received from TNO, was also used by measurements performed at TNO. So it was not obvious if the difference was caused by the slightly worn tyre. Therefore some experiments are performed with a new tyre as well to see if that has some influence on the tyre behaviour earlier discovered. These findings, the difference between the old and new tyre and the results of measuring with a positive and a negative camber angle, are also discussed in this chapter.

4.1 Results non-lagging effect

First, the results of the three different loading conditions, concerning the non-lagging lateral force, the steady-state side force and the steady-state vertical force will be discussed. In figure 4.1 an overview of these results for positive and negative camber angles is depicted. Measurement of type 37Z is only conducted with negative camber angles, because it was not possible to reach a positive camber angle of 15 degrees due to the limitation in rotating the measuring hub.
From the results of the non-lagging lateral force, depicted in the left figures, it can be concluded that the level of instantaneously developed non-lagging part is very depended on the loading case. For the loading case where the cambered wheel is vertically loaded against the road (37Z), the amount of non-lagging lateral force is smaller than for the two other loading conditions. The results also show that the non-lagging forces approximately correspond for positive and negative camber angles. The vertical load is less important for the non-lagging part; a slight increase in non-lagging lateral force occurs for an increasing vertical load.
The results of the steady-state vertical force of measurement 38C do not show a constant level for an increasing camber angle. Because the track is cambered after the tyre is loaded against the track, an increase in vertical force occurs, which is shown in the right figure. The two other loading conditions show an almost constant level of steady-state vertical force for an increasing camber angle.
From the results of the steady-state side force it can be concluded that for negative camber angles the values of the steady-state side force correspond; only measurement 38C differs as a result of the increasing vertical load. For positive camber angles a difference occurs in the reached level of steady-state side force for the different loading conditions. For measurement of type 38R the largest difference occurs between positive and negative camber angles. Observing the results, for positive camber angles the steady-state side force is about 25 percent lower than for negative angles.
The non-lagging tyre behaviour for car tyres is already investigated by Pacejka and Higuchi and the results are described in (Pacejka, 2002). From these results it can be concluded that for some loading conditions the non-lagging side force acts in a direction opposite to the steady-state side force. Observations of the results for motorcycles tyres show that the initial non-lagging lateral force always acts in a direction equal to the steady-state side force.
From the results the non-lagging part fraction for motorcycle tyres is determined to characterize the non-lagging behaviour. In figure 4.2 the results of the non-lagging part fraction (ε_{NL}) for positive and negative camber angles are presented.

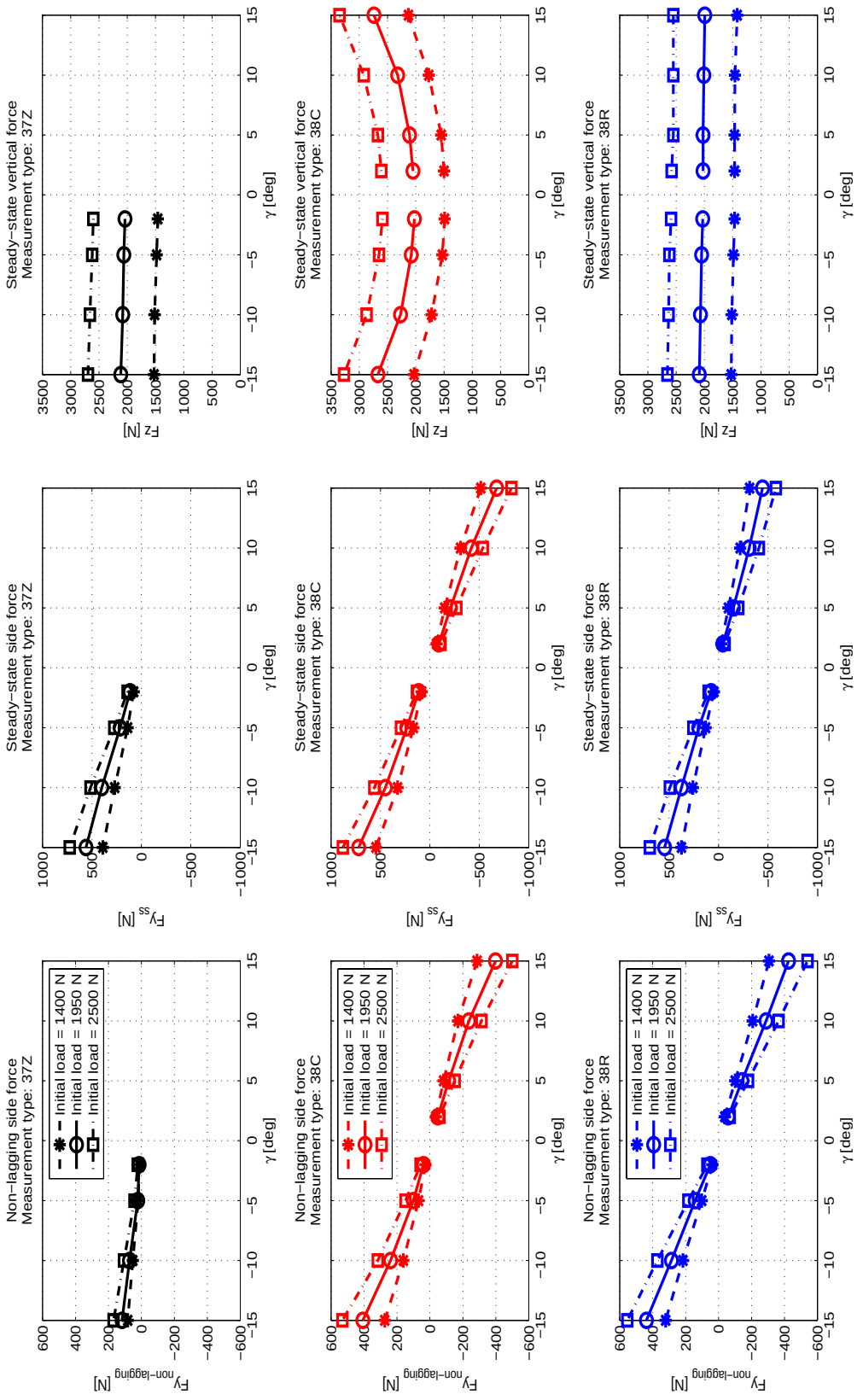

Fig. 4.1 Overview of the non-lagging and steady-state side force and the steady-state vertical load

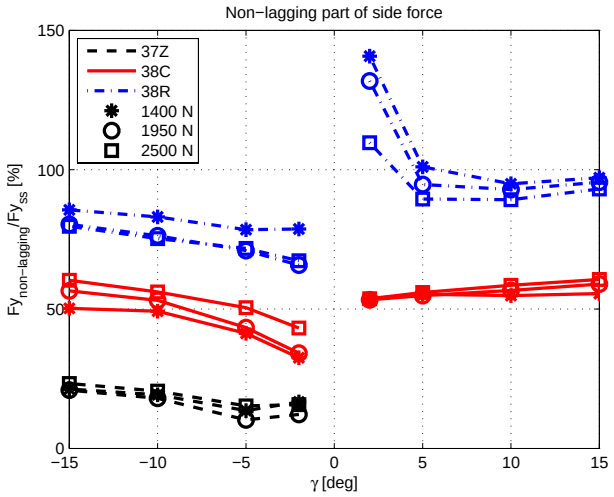

Fig. 4.2 Non-lagging part of side force response for the three different loading conditions

This figure gives the percentage of the non-lagging part with respect to the steady-state side force for the three different loading conditions, determined with the non-lagging part fraction as defined in chapter 1. No results for measurement of type 37Z are depicted for positive camber angles, because it was not possible to measure with positive camber angles as mentioned before.
From the results it can be observed that several differences occur between the measurements with positive and negative camber angles. The main difference between the measurements is caused by the different loading processes. The load case of the tyre is different for the three measurements and therefore the development of the forces and moments is different. This results in a different non-lagging part fraction for the three loading cases. The second observation clarifies that the magnitude of the vertical force is less important than the loading case. For a load case the magnitude of the non-lagging part fraction is approximately of the same level for the several loading conditions. For an increasing camber angle, the non-lagging part fraction shows a slightly increasing behaviour.
As already observed in the results from figure 4.1, differences occur between the measurements with a positive or a negative camber angle. Observations of the results of measurement of type 38R for positive camber angles show a significant difference with the results for negative camber angles. For small camber angles (γ=2 degrees) the non-lagging lateral force is higher than the steady-state side force. This results in a non-lagging part ratio larger than 100 percent. For larger camber angles the steady-state side force is approximately equal to the non-lagging side force, which results in a non-lagging part ratio of approximately 100 percent. These observations deviate a lot from the results with negative camber angles. This phenomenon should not be expected, for both positive and negative camber angles it is preferred to develop the same level of steady-state side force. The appearance of this phenomenon can be caused by asymmetric tyre behaviour while cornering or by an inaccuracy of the measuring hub from the Flat Plank Tyre Tester. To further investigate the observed differences, measurements have been performed with a new tyre of the same type as the old tyre that was delivered by TNO. The results of the measurements with the new tyre and a comparison between the old and new tyre are described in the next section.

4.2 Discussion of the results between the old and new tyre

For the comparison between the old and new tyre, measurements have been performed for the different loading conditions. For the comparison measurements a data selection is made under which conditions the measurements are performed. The overview of this selection is given below:

Measurement conditions for the new tyre:

- Nominal load: 1950 N
- Camber angle: -5 and 5 degrees
- Measurement types: 37Z, 38C and 38R

In figure 4.3 through 4.5 the results of these measurements are presented.

Measurement 37Z:

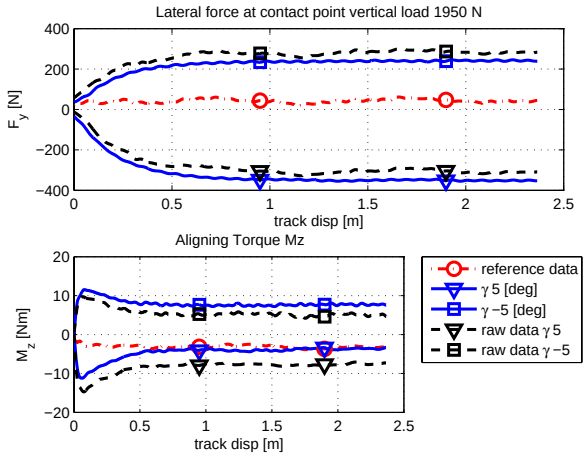

	γ = -5	γ = 5
$F_{y,ss}$	240 N	-348 N
$F_{y,NL}$	37 N	-34 N
$M_{z,ss}$	7.5 Nm	-4 Nm

Fig. 4.3 Results new tyre measurements for case 37Z

Measurement 38C:

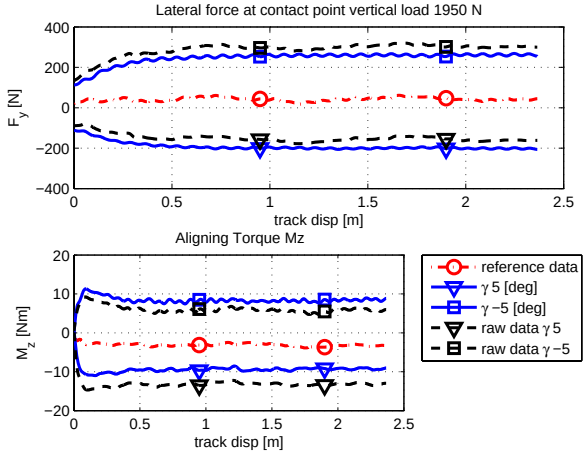

	γ = -5	γ = 5
$F_{y,ss}$	260 N	-200 N
$F_{y,NL}$	113 N	-111 N
$M_{z,ss}$	8.3 Nm	-9 Nm

Fig. 4.4 Results new tyre measurements for case 38C

Measurement 38R:

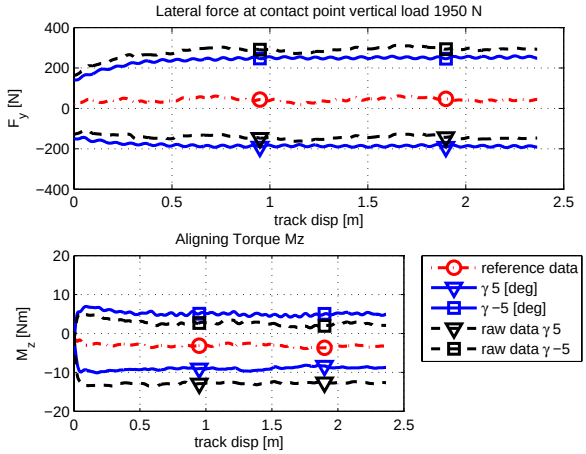

	$\gamma = -5$	$\gamma = 5$
$F_{y,ss}$	250 N	-185 N
$F_{y,NL}$	142 N	-149 N
$M_{z,ss}$	5 Nm	-9 Nm

Fig. 4.5 Results new tyre measurement for case 38R

From the measurements with the new tyre it can be concluded that this tyre shows the same tyre behaviour as discovered with the old tyre. Differences occur in the steady-state results for positive and negative camber angles. For negative camber angles the three measurements exhibit the same tyre behaviour. The magnitude of the steady-state side force values correspond for these experiments. However, for the measurements with a positive camber angle several differences occur between the measurements. These differences mainly occur in the development of the side force and the reached level of steady-state side force. For measurement of type 37Z (see figure 4.3) the steady-state side force for positive camber angles is higher than the steady-state level for negative camber angles. For the measurements where the track of the Flat Plank Tyre Tester is cambered (see figure 4.4 and 4.5) the opposite behaviour occurs. Here the steady-state force is lower than for negative camber angles. This phenomenon was also recognized in the measurements with the old tyre. The instantaneously developed non-lagging part for a specific load case corresponds for positive and negative angles. When the tyre starts rolling the side force develops to a different level of steady-state side force, while it is cambered with a negative or positive angle. This is not a desired behaviour for motorcycle tyres, because it means that during cornering the developing of side force is different for both sides. This will lead to an unnatural experience while driving through a corner, because more side force is developed in a direction at a certain inclination angle.
From the measurement results of the new tyre, the non-lagging part fraction for the different loading cases is determined. Subsequently, a comparison between the old and new tyre, for the measurement conditions of the new tyre, is made. These results are depicted in figure 4.6. The data point for measurement 37Z with a positive camber angle of the old tyre is not present, because this measurement is not performed with the old tyre.

Observations of the results of the non-lagging part fractions show that the occurred tyre behaviour, as a result of the steady-state differences, also arises in the non-lagging part fractions. For positive and negative camber angles, different non-lagging part fractions occur. The measurements 38C and 38R show higher fractions, caused by lower levels of steady-state side forces for positive camber angles. Measurement 37Z has a slightly lower fraction for positive camber angles, as a result of the higher level of steady-state side force for these angles. For a specific load case the fractions are approximately of the same magnitude, only for measurement of type 38R the fractions of the new tyre are approximately 20 percent lower than for the old tyre.

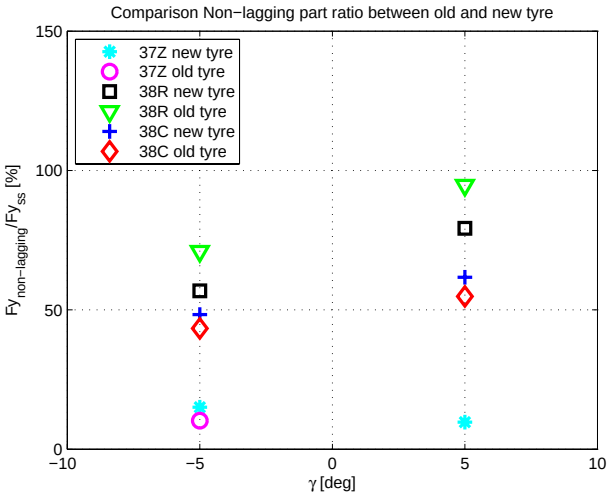

Fig. 4.6 Overview of the non-lagging part fractions for the old and new tyre

Two possible explanations for the appearance of the differences between the measurements with a positive or a negative camber angle are given. It is possible that the measuring hub of the Flat Plank Tyre Tester is the cause of the differences. To investigate if the measuring hub measures the same level of lateral force in both sign directions, slip angle experiments are executed in both directions of travel of the road. The results of these measurements are discussed in Appendix III. From the results it can be concluded that the measuring hub is not responsible for the differences between the camber measurements with positive and negative angles. A slight difference occurs in the level of lateral force, but it is certainly not of the magnitude observed during the camber measurements. The other explanation could be that the tyre has an asymmetric build of the different layers of the tyre and therefore shows differences while cornering. As mentioned before, this is not a behaviour that would be expected for motorcycle tyres. At this moment it is a bit inexplicable why this tyre behaviour occurs while cornering, because there are not any reference measurements with other types of motorcycle tyres. It is not possible to conclude that this behaviour is the same for every motorcycle tyre.

All measurements performed during the internal traineeship to investigate the non-lagging effect and tyre behaviour for motorcycle tyres are included in Appendix V.

5 Conclusions and recommendations

In this report the non-lagging effect of motorcycle tyres is studied experimentally. A description of the measurements is given, which have been performed to determine the non-lagging and steady-state behaviour. Also measurements have been performed, which can be used to determine the parameters for building a tyre model. In the last part of the report the results of the camber measurements have been discussed. Emphasize in the discussion is laid on the non-lagging effect and developing of steady-state side force.

Conclusions:

- The loading case of the tyre has the most influence on the contribution of the non-lagging side force, which is developed directly after the wheel is cambered and loaded.
- The magnitude of the vertical load is less important than the loading case of the tyre. For a specific loading case, the non-lagging part fractions approximately correspond with each other for the several vertical loads.
- The non-lagging effect for motorcycle tyres differ from that for car tyres. The initial non-lagging side force that occurs, always acts in a direction equal to the steady-state side force.
- For an increasing camber angle, the non-lagging part fraction shows a slightly increasing behaviour. This increasing behaviour is not dependent of the vertical load; for the three vertical loads it shows approximately the same increase.

During the experimental study of the non-lagging behaviour of the tyre studied, it appears that a difference occurs between measurements with a positive or negative camber angle.

- A general phenomenon that occurs for the studied motorcycle tyre is that the steady-state side force for the several loading conditions does not correspond. This phenomenon should not be expected, since for both positive and negative camber angles it is preferred to develop the same level of steady-state side force.
- The measurement of type 38R with small positive camber angles ($\gamma = 2$ degrees) shows a significant difference with the results for negative camber angles. The non-lagging lateral force is higher than the steady-state side force. This result in a non-lagging part fraction larger than 100 percent.

To investigate this observed tyre behaviour further, more measurements have been performed with a brand new tyre of the same type. Experiments consist of measurements with the three loading cases for a positive and negative camber angle of 5 degrees. From the results it can be concluded that:

- The results of the new tyre show the same tyre behaviour as discovered with the old tyre. Differences occur in the steady-state results for positive and negative camber angles. For negative camber angles the three measurements exhibit the same tyre behaviour. The magnitude of the steady-state side force values correspond for these experiments.
- The non-lagging part for measurements with the new tyre corresponds with the non-lagging part of the old tyre.
- For the measurements with a positive camber angle several differences occur in the development of the side force and the reached level of steady-state side force. For measurement of type 37Z the steady-state side force for positive camber angles is higher than the steady-state level for negative camber angles. For the

measurements where the track of the Flat Plank Tyre Tester is cambered the opposite behaviour occurs. Here the steady-state force is lower than for negative camber angles.
- For positive and negative camber angles, different non-lagging part fractions occur as a result of the different levels of steady-state side force for the loading cases.

Recommendations:

In this experimental study of the non-lagging effect of motorcycle tyres only one type of a motorcycle tyre is tested on the Flat Plank Tyre Tester. From the results of these experiments it can be concluded that some interesting phenomenon occur during cambering of the tyre. It is difficult to give an overall conclusion of the non-lagging tyre behaviour of motorcycle tyres, so the following recommendations can be considered for further research:

- To further investigate the non-lagging tyre behaviour, more camber measurements have to be performed with several motorcycle tyres of different type. Emphasize in this investigation should be laid on:
    - Different loading cases. It appears that the loading case has the most influence on the non-lagging part and the development of the side forces.
    - Differences between measuring with a positive or a negative camber angle.
- From the measurement results determine the parameters necessary to build the semi-empirical tyre model used for car tyres to predict the non-lagging part.
- Validate if this existing tyre model (used for car tyres) also predicts the non-lagging part of motorcycle tyres.

References

Besselink, I.J.M. (2002), Lecture notes Vehicle Dynamics (4L150), Eindhoven University of Technology, Eindhoven, The Netherlands 2003

Blom, R.E.A. and Vissers, J.P.M. and Merkx, L.L.F. (2004), Manual for the Flat Plank Tyre Tester, internal report, Eindhoven University of Technology, Eindhoven, The Netherlands, report number DCT2004.XX, 2004

Higuchi, A. (1997a), Transient Response of Tyres at Large Wheel Slip and Camber, doctoral thesis, University of Technology, Delft, The Netherlands, ISBN 90-407-1563-7, 1997

Higuchi, A. (1997b), Experimental study on transient response of tyres, internal report, University of Technology, Delft, The Netherlands, report number 97.3.VT.4891, 1997

Pacejka, H.B. (2002), Tyre and Vehicle Dynamics, Butterworth-Heinemann, London, United Kingdom, ISBN 0-7506-5141-5, 2002

Pacejka, H.B. (2004), Spin: Camber and turning, The third wheel slip input quantity, Presentation sheets from 3D Tyre Colloquium, Vienna, Austria 2004

Schmeitz, A.J.C. (2004), A Semi-Empirical Three-Dimensional Model of the Pneumatic Tyre Rolling over Arbitrarily Uneven Road Surfaces, doctoral thesis, University of Technology, Delft, The Netherlands, ISBN 90-9018380-9, 2004

Verkerk, W.S. (2003), Flatplank experimenten voor de ontwikkeling van een 3D bandmodel, internal report, University of Technology, Delft, The Netherlands, report number VT.6775, 2003

Zegelaar, P.W.A. (1998), The Dynamic Response of Tyres to Brake Torque Variations and Road Unevennesses, doctoral thesis, University of Technology, Delft, The Netherlands, ISBN 90-370-0166-1, 1998

Appendix I

Derivation of the right-handed axis system in the tyre contact centre

A rotation about the x-axis of the contact patch coordinate system occurs because of cambering of the tyre. This rotation is indicated with γ and is the camber angle of the tyre. To calculate the forces at the contact patch the rotation matrix $\underline{R}$ for a rotation about the x-axis is used. In this derivation $\underset{\sim}{\vec{e}}^{w}$ is the wheel axis system, which corresponds with the axis system at the contact centre. The axle axis system is $\underset{\sim}{\vec{e}}^{a}$ and this corresponds with the axis system of the wheel axle. In this appendix the derivation of the forces and moments for a rotation about the x-axis is made.

Forces equilibrium:

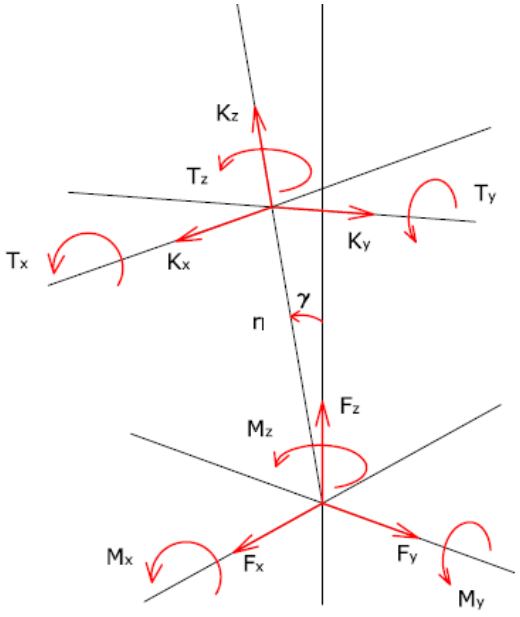

$$\underset{\sim}{\vec{e}}^{w} = \underline{R}\,\underset{\sim}{\vec{e}}^{a}$$

$$\underset{\sim}{\vec{e}}^{w^T} = \underset{\sim}{\vec{e}}^{a^T}\underline{R}^T$$

$$\underset{\sim}{\vec{e}}^{w^T}\underline{R} = \underset{\sim}{\vec{e}}^{a^T}\underbrace{\underline{R}^T\underline{R}}_{\underline{I}}$$

$$\underset{\sim}{\vec{e}}^{w^T}\underline{R} = \underset{\sim}{\vec{e}}^{a^T}$$

$$\underline{R} = \begin{bmatrix} 1 & 0 & 0 \\ 0 & \cos\gamma & -\sin\gamma \\ 0 & \sin\gamma & \cos\gamma \end{bmatrix}$$

$$\vec{F} = \begin{bmatrix} F_x & F_y & F_z \end{bmatrix}\underset{\sim}{\vec{e}}^{w} = \begin{bmatrix} K_x & K_y & K_z \end{bmatrix}\underset{\sim}{\vec{e}}^{a}$$

$$\underset{\sim}{\vec{e}}^{w^T}\begin{bmatrix} F_x \\ F_y \\ F_z \end{bmatrix} = \underset{\sim}{\vec{e}}^{w^T}\begin{bmatrix} 1 & 0 & 0 \\ 0 & \cos\gamma & -\sin\gamma \\ 0 & \sin\gamma & \cos\gamma \end{bmatrix}\begin{bmatrix} K_x \\ K_y \\ K_z \end{bmatrix}$$

$$\begin{bmatrix} F_x \\ F_y \\ F_z \end{bmatrix} = \begin{bmatrix} K_x \\ K_y\cos(\gamma) - K_z\sin(\gamma) \\ K_y\sin(\gamma) + K_z\cos(\gamma) \end{bmatrix}$$

Moment equilibrium about wheel centre:

$$\underset{\sim}{\vec{e}}^{a^T}\begin{bmatrix} T_x \\ T_y \\ T_z \end{bmatrix} = \underset{\sim}{\vec{e}}^{w^T}\begin{bmatrix} M_x \\ M_y \\ M_z \end{bmatrix} + \vec{r}\times\vec{F}$$

$$\underset{\sim}{\vec{e}}^{a^T}\begin{bmatrix} T_x \\ T_y \\ T_z \end{bmatrix} = \underset{\sim}{\vec{e}}^{w^T}\begin{bmatrix} M_x \\ M_y \\ M_z \end{bmatrix} + \underset{\sim}{\vec{e}}^{a^T}\begin{bmatrix} 0 \\ 0 \\ -r_l \end{bmatrix} \times \underset{\sim}{\vec{e}}^{a^T}\begin{bmatrix} K_x \\ K_y \\ K_z \end{bmatrix}$$

$$\underset{\sim}{\vec{e}}^{a^T}\begin{bmatrix}T_x\\T_y\\T_z\end{bmatrix}-\underset{\sim}{\vec{e}}^{a^T}\left\{\begin{bmatrix}0\\0\\-r_l\end{bmatrix}\times\begin{bmatrix}K_x\\K_y\\K_z\end{bmatrix}\right\}=\underset{\sim}{\vec{e}}^{w^T}\begin{bmatrix}M_x\\M_y\\M_z\end{bmatrix}$$

$$\underset{\sim}{\vec{e}}^{w^T}\underline{R}\begin{bmatrix}T_x\\T_y\\T_z\end{bmatrix}-\underset{\sim}{\vec{e}}^{w^T}\underline{R}\left\{\begin{bmatrix}0\\0\\-r_l\end{bmatrix}\times\begin{bmatrix}K_x\\K_y\\K_z\end{bmatrix}\right\}=\underset{\sim}{\vec{e}}^{w^T}\begin{bmatrix}M_x\\M_y\\M_z\end{bmatrix}$$

$$\begin{bmatrix}M_x\\M_y\\M_z\end{bmatrix}=\begin{bmatrix}T_x-r_lK_y\\T_y\cos(\gamma)-T_z\sin(\gamma)+K_xr_l\cos(\gamma)\\T_y\sin(\gamma)+T_z\cos(\gamma)+K_xr_l\sin(\gamma)\end{bmatrix}$$

Appendix II

Calibration LVDT

Due to carelessness and incorrect use of the LVDT during previous measurements, it is not clear if the LVDT still works correctly. Therefore the LVDT is first calibrated. If necessary the amplification ratio in Labview will be corrected. The amplification ratio is necessary to determine the vertical displacement of the measuring hub (and rack).

Calibration method:
Determine range of LVDT and compare this with position of rack.

Voltage range LVDT: 0 -10 Volt
Position range rack: 138 – 53 mm (displacement: 0 – 85 mm)
Amplification ratio [k]: 8.1334

Divide position range rack in steps of 5 mm.
Measure output voltage LVDT at each step.
For that purpose we branch off the output voltage signal in Labview.
Plot the output voltage LVDT vs. the rack displacement using Matlab. (Fig. A2.1)
Put a linear fit over data plot and determine equation.
Use the equation of the fit to determine amplification ratio.

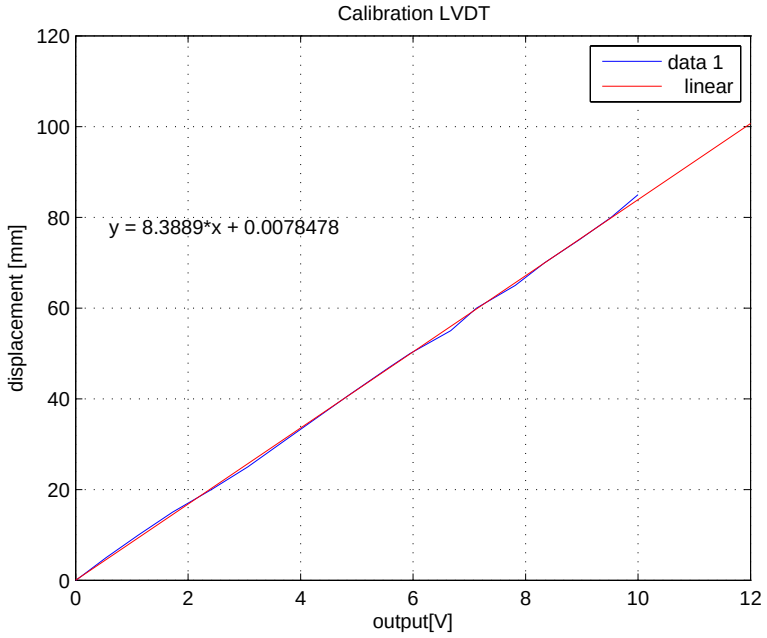

Fig. A2.1, Calibration LVDT

Conclusion of the calibration is that the amplification ratio should be $k = 8.3889$ instead of 8.1334. The ratio is corrected in the Labview program of the Flat Plank Tyre Tester.

Appendix III

Slip angle measurement for checking lateral force at measuring hub

This measurement is performed to exclude the fact that there is a problem with the measuring hub. An experiment with a slip angle of five and minus five degrees is performed on the Flat Plank Tyre Tester. During this experiment the track of the Flat Plank Tyre Tester is used in both directions of travel. When a slip angle experiment is performed in both directions of travel, the results of a measurement with five and minus five degrees should give the same magnitude of side force. This is caused by the fact that the sign of the side force will change in the opposite direction, when the direction of travel of the track is changed.

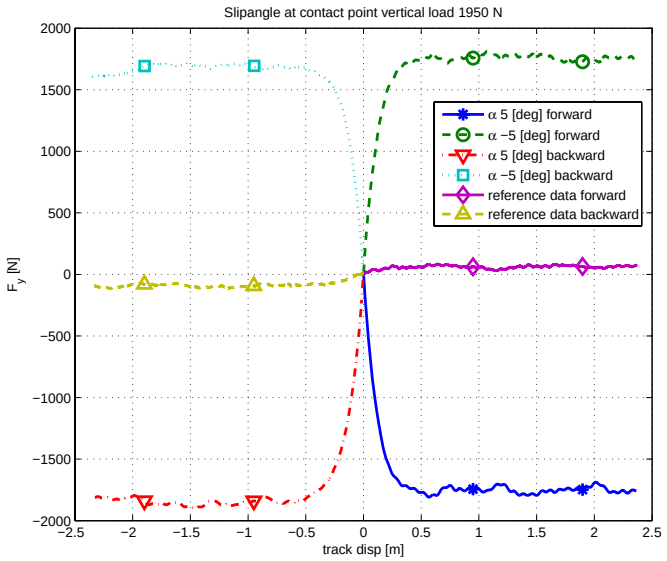

Fig. A3.1, Results slip angle experiment

Slipangle [deg]	Direction	Fy,ss [N]
5	forward	1780
-5	forward	-1750
5	backward	1700
-5	backward	-1870

From the results it can be concluded that the difference between a measurement performed in forward and backward direction is approximately 50-90 N. These differences are smaller than the results of the camber measurements. So it can be concluded that the measuring hub is not responsible for the differences, which occurs in the camber measurements.

Appendix IV

Description measurement files

Reference measurement:

Filename:	refl1950acp1
ref	indication reference measurement
l1950	indication vertical load (1400, 1950, 2500 N)
ac	constant axle height
p1	indication position on tyre (p1,p2,p3)

Camber measurements:

Filename:	cam05pl1950ac37Zp1
cam	indication camber measurement
05	camber angle (02, 05, 10, 15 degrees)
p	indication camber angle (positive or negative)
l1950	indication vertical load (1400, 1950, 2500 N)
ac	constant axle height
37Z	indication measurement type (37Z, 38C, 38R)

Stiffness measurements:

Filename	vert_stiffness_p1
vert_stiffness_	indication vertical stiffness measurement
p1	indication position on tyre (p1, p2, p3) for static measurement or (roll) for rolling measurement

Filename	latstiffl1950s100p1
latstiff	indication lateral stiffness measurement
l1950	vertical load (1400, 1950, 2500 N)
s100	sample frequency adjusted on 100 Hz
p1	indication position on tyre (p1, p2, p3)

Relaxation measurements

Filename	rel_l1950a0p1
rel_	indication relaxation measurements
l1950	vertical load (1400, 1950, 2500 N)
a0	indication slip angle (0 or 1 degrees)
p1	position on tyre (p1, p2, p3)

Measurements new tyre:

Filename	newtyrecam05pl1950ac37Zp1
newtyre	indication measurements with new tyre
cam	indication camber measurements
05	camber angle (02, 05, 10, 15 degrees)
l1950	vertical load (1400, 1950, 2500 N)
ac	constant axle height
37Z	indication measurement type (37Z, 38C, 38R)

Appendix V

Overview of the performed measurements in this study

Measurement 37Z (negative camber angles):

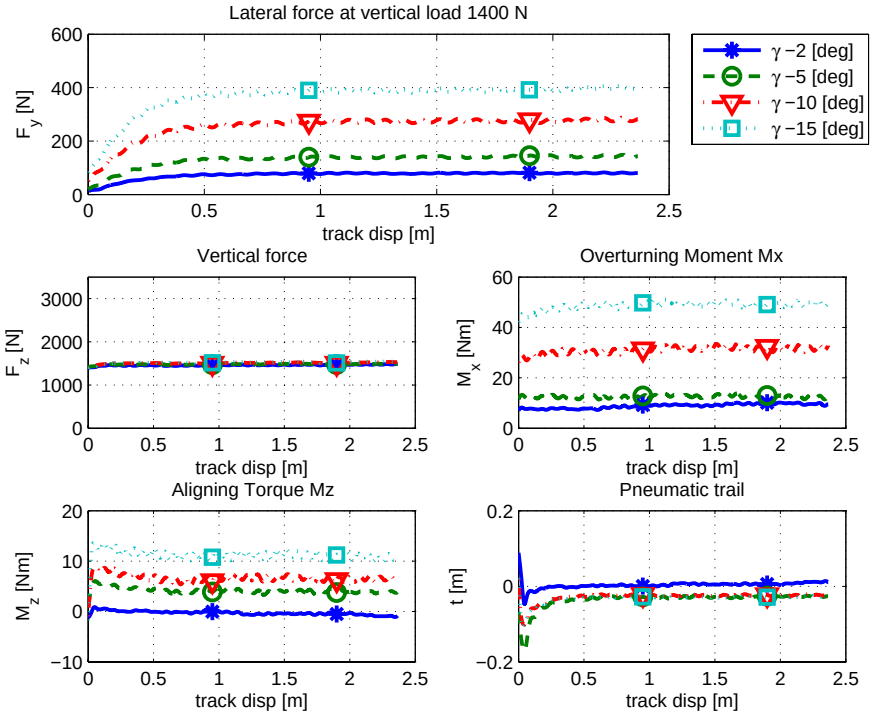

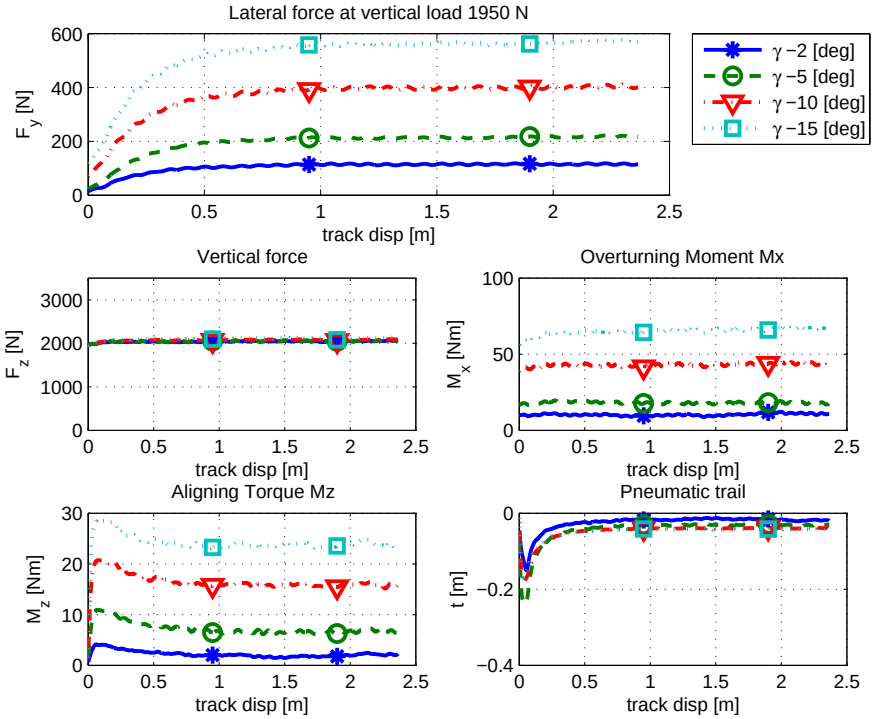

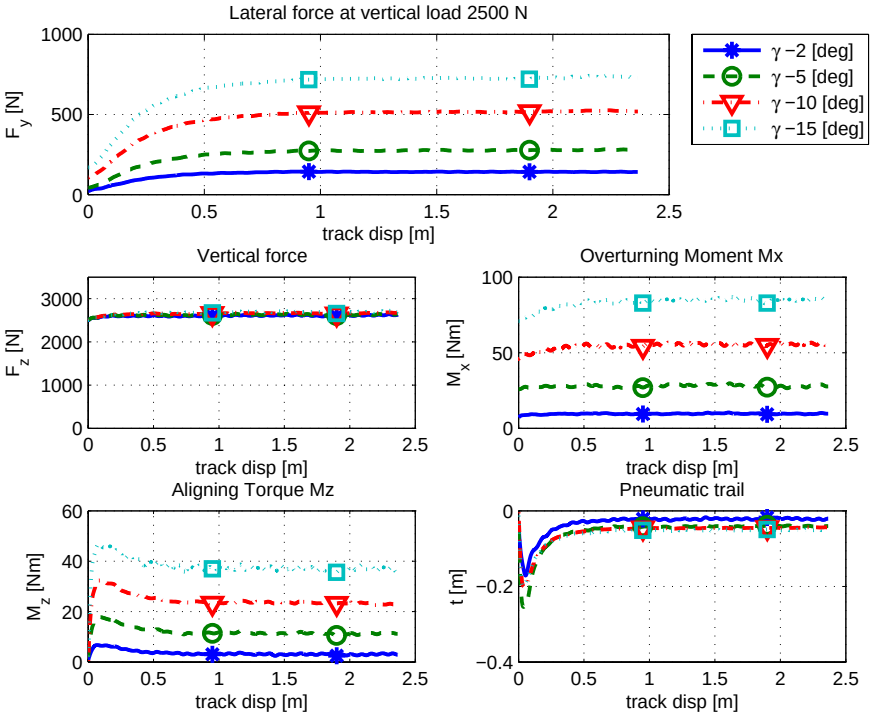

Measurement 38C (negative camber angles):

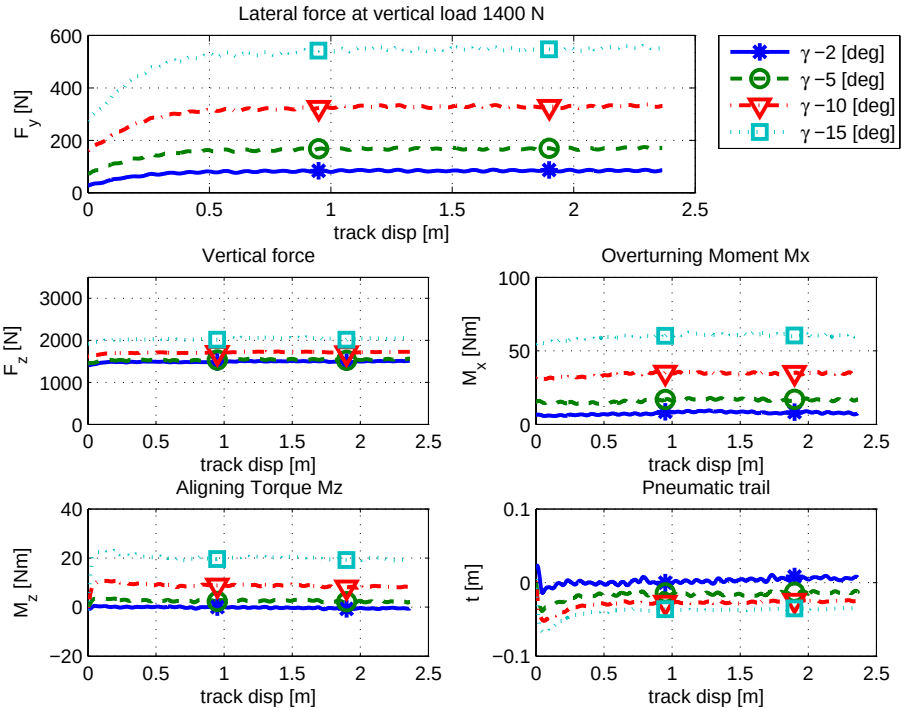

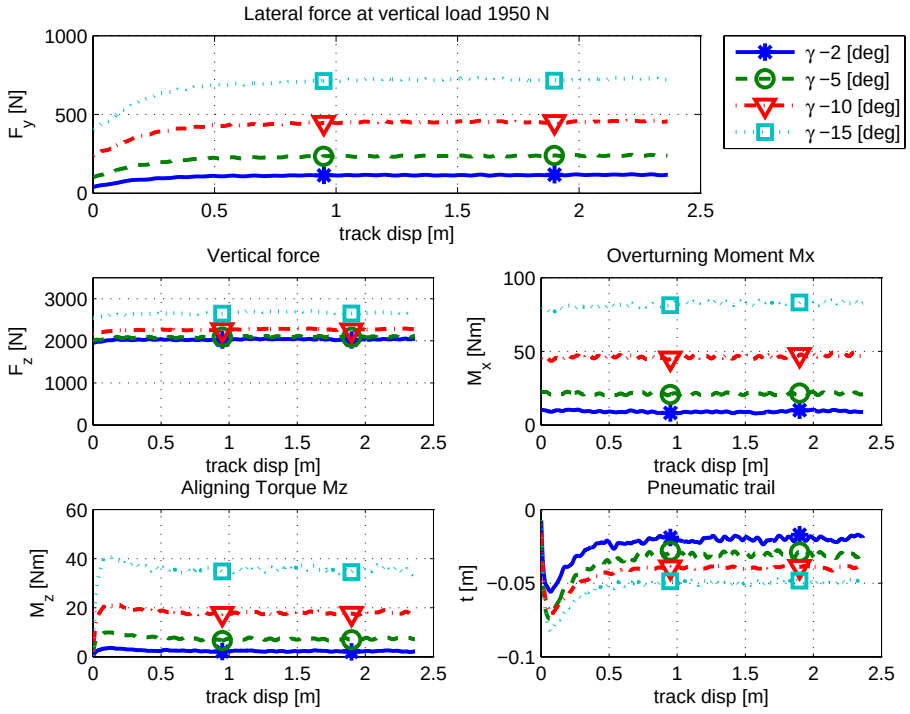
Lateral force at vertical load 1950 N
F_y [N]
track disp [m]
γ −2 [deg]
γ −5 [deg]
γ −10 [deg]
γ −15 [deg]
Vertical force
F_z [N]
track disp [m]
Overturning Moment Mx
M_x [Nm]
track disp [m]
Aligning Torque Mz
M_z [Nm]
track disp [m]
Pneumatic trail
t [m]
track disp [m]

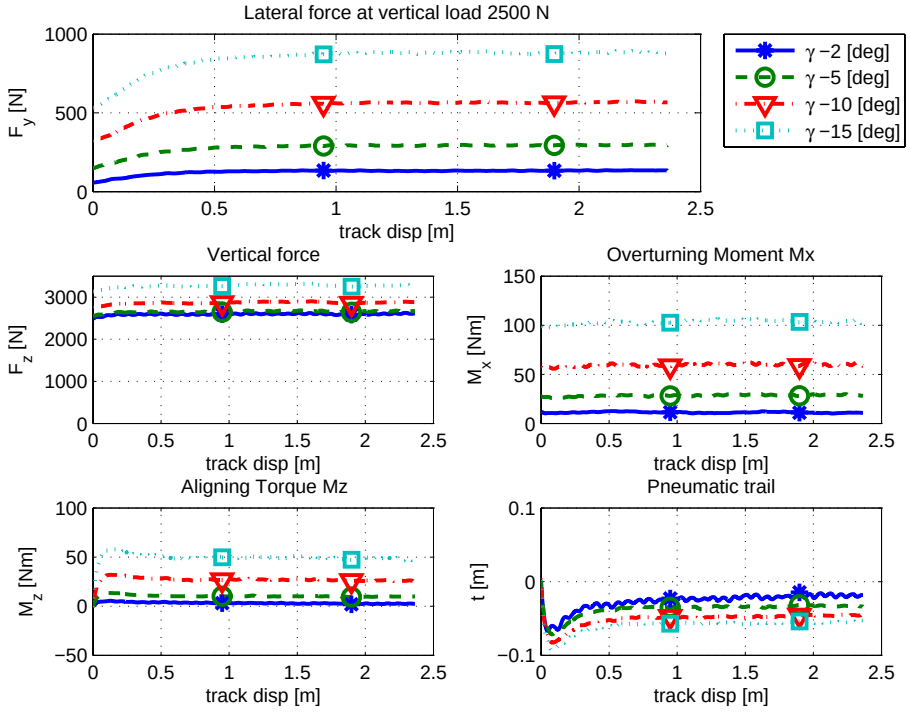
Lateral force at vertical load 2500 N
F_y [N]
track disp [m]
γ −2 [deg]
γ −5 [deg]
γ −10 [deg]
γ −15 [deg]
Vertical force
F_z [N]
track disp [m]
Overturning Moment Mx
M_x [Nm]
track disp [m]
Aligning Torque Mz
M_z [Nm]
track disp [m]
Pneumatic trail
t [m]
track disp [m]

Measurement 38C (positive camber angles):

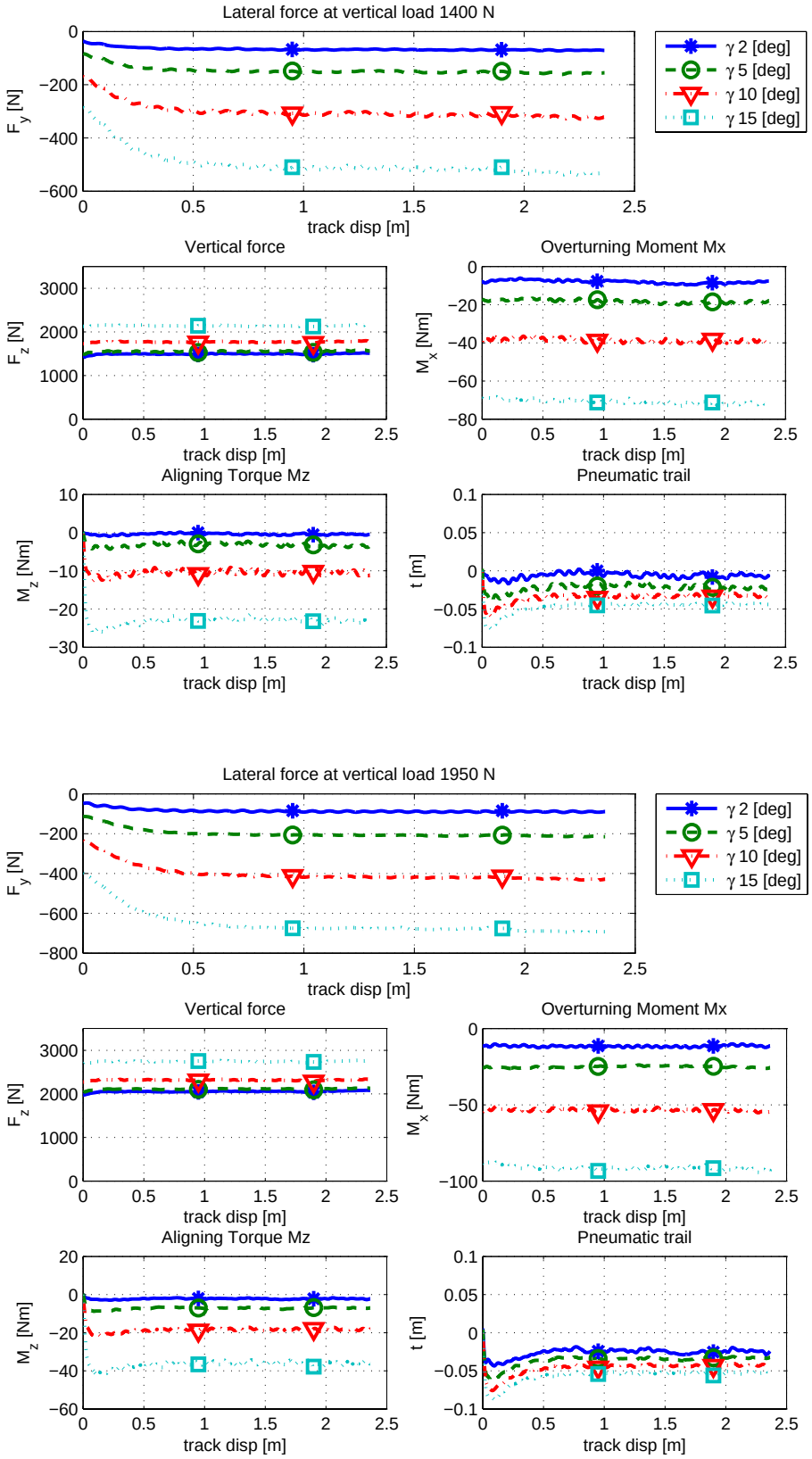

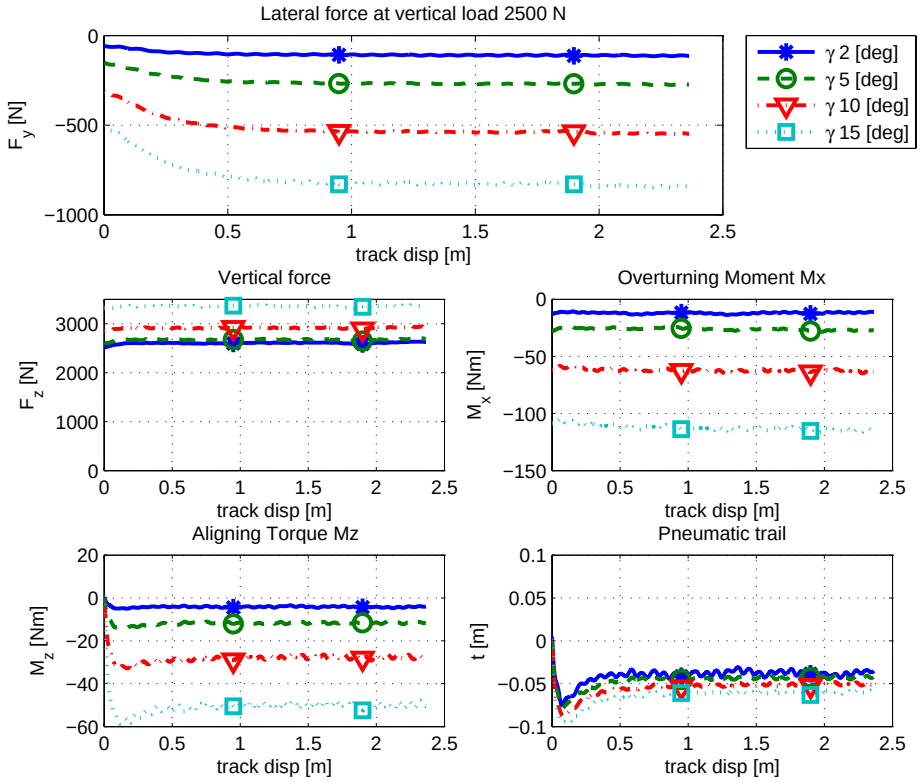

Measurement 38R (negative camber angles):

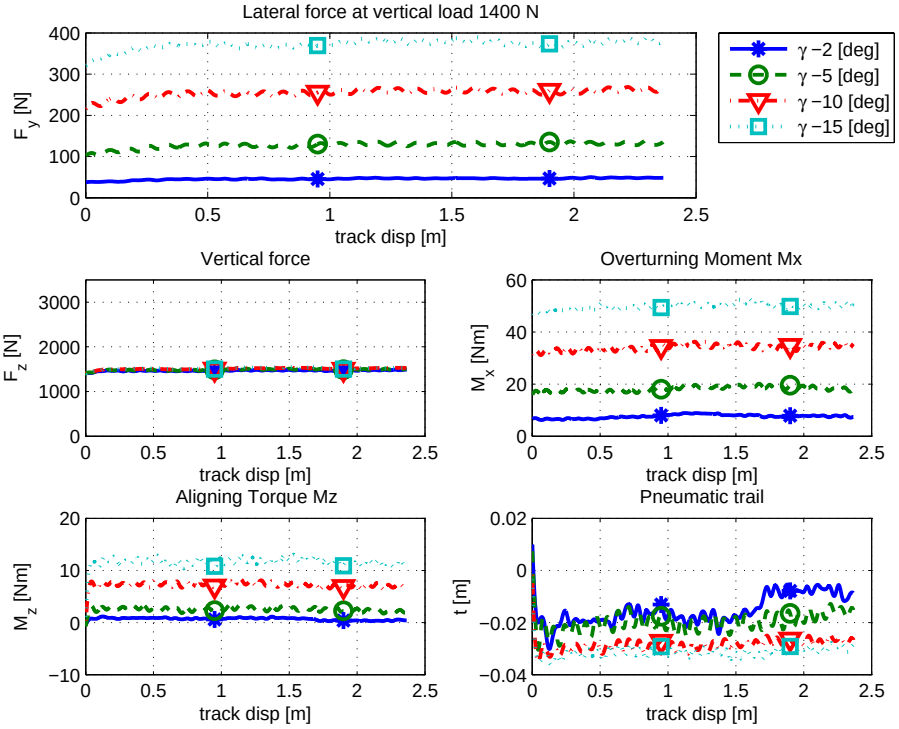

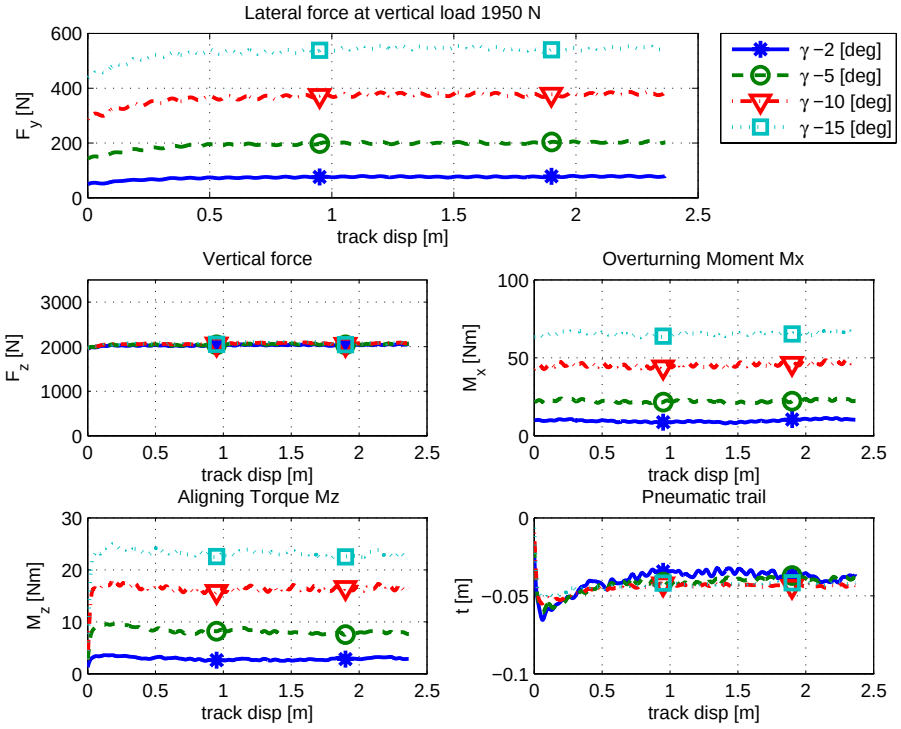
Lateral force at vertical load 1950 N
F_y [N]
track disp [m]
γ −2 [deg]
γ −5 [deg]
γ −10 [deg]
γ −15 [deg]
Vertical force
F_z [N]
track disp [m]
Overturning Moment Mx
M_x [Nm]
track disp [m]
Aligning Torque Mz
M_z [Nm]
track disp [m]
Pneumatic trail
t [m]
track disp [m]

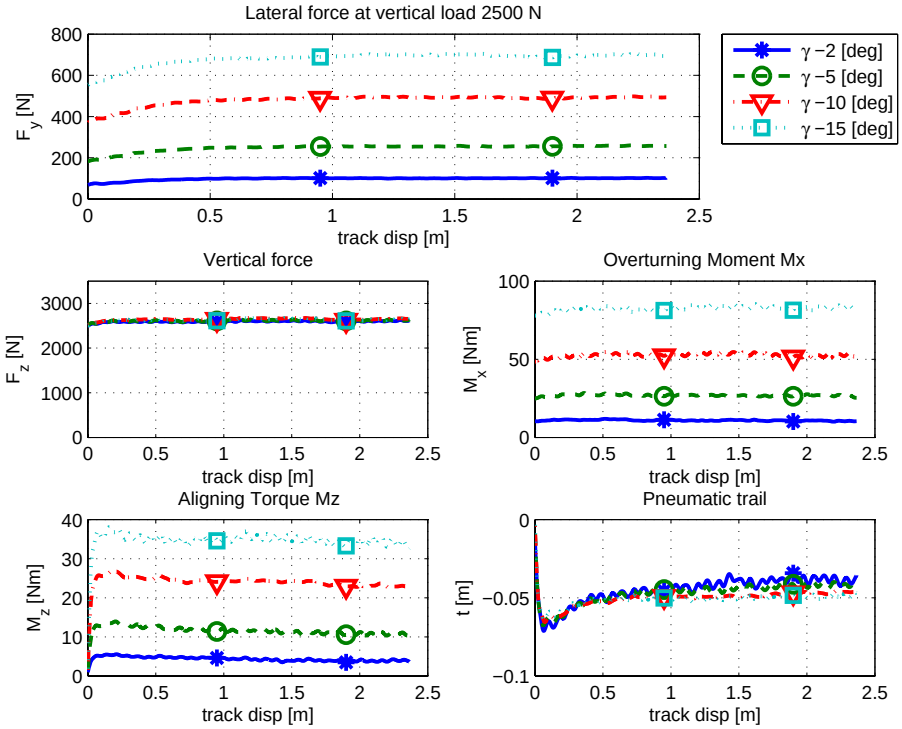
Lateral force at vertical load 2500 N
F_y [N]
track disp [m]
γ −2 [deg]
γ −5 [deg]
γ −10 [deg]
γ −15 [deg]
Vertical force
F_z [N]
track disp [m]
Overturning Moment Mx
M_x [Nm]
track disp [m]
Aligning Torque Mz
M_z [Nm]
track disp [m]
Pneumatic trail
t [m]
track disp [m]

Measurement 38R (positive camber angles):

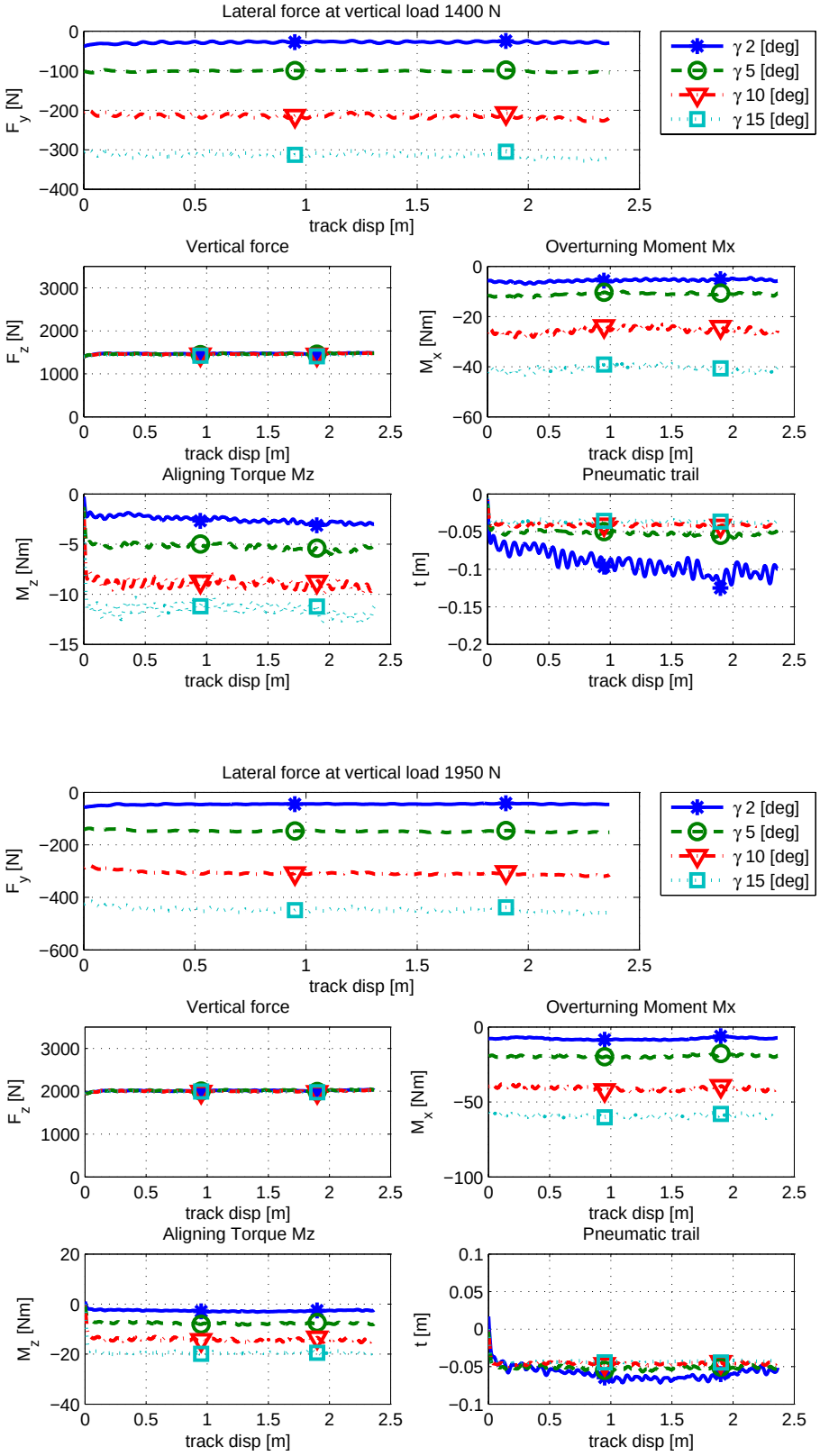

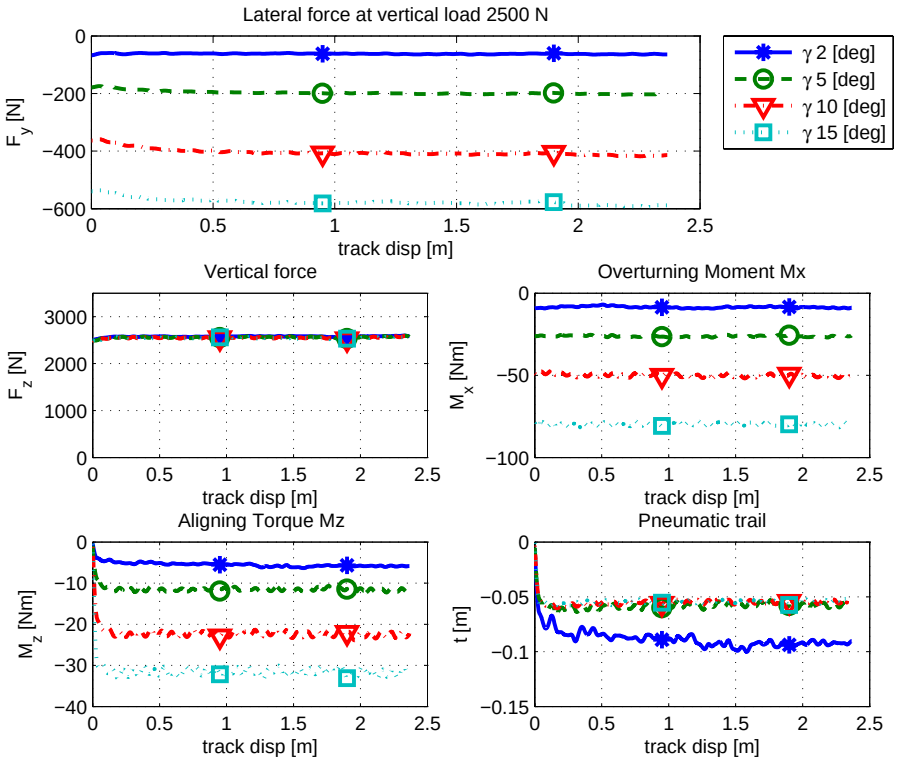

Results measurements new tyre with camber angles of -5 and 5 degrees:
Measurement 37Z:

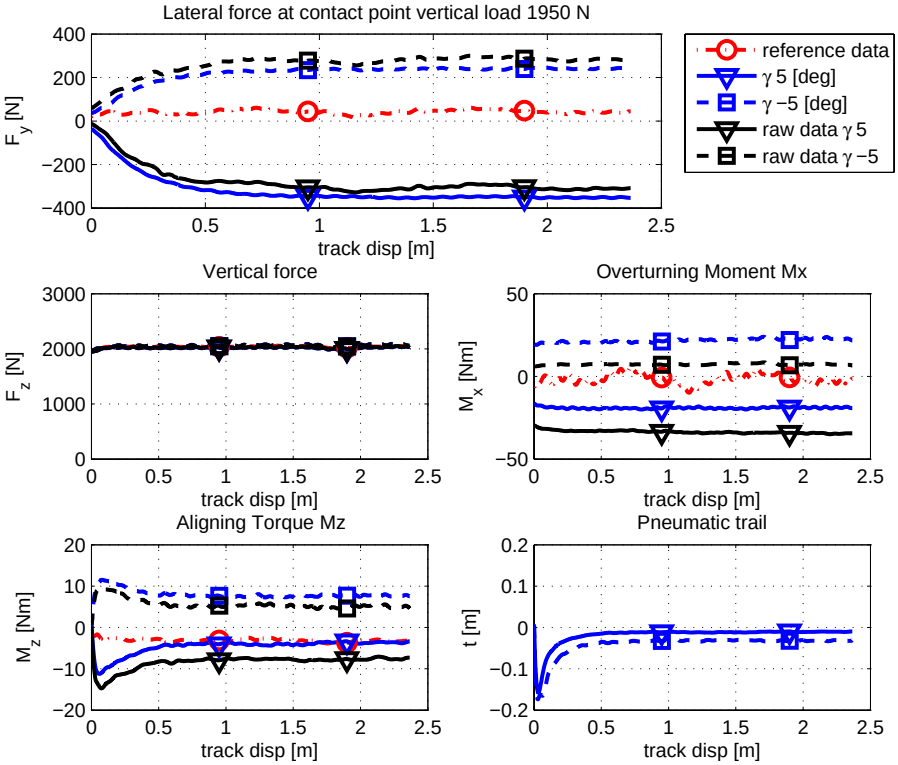

Measurement 38C:

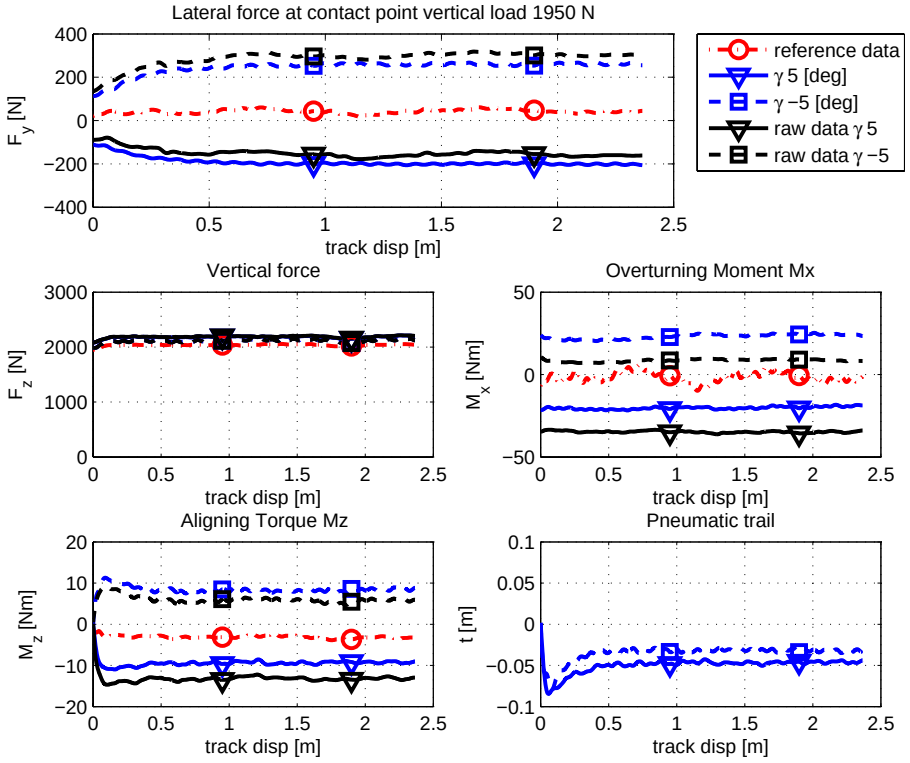

Measurement 38R:

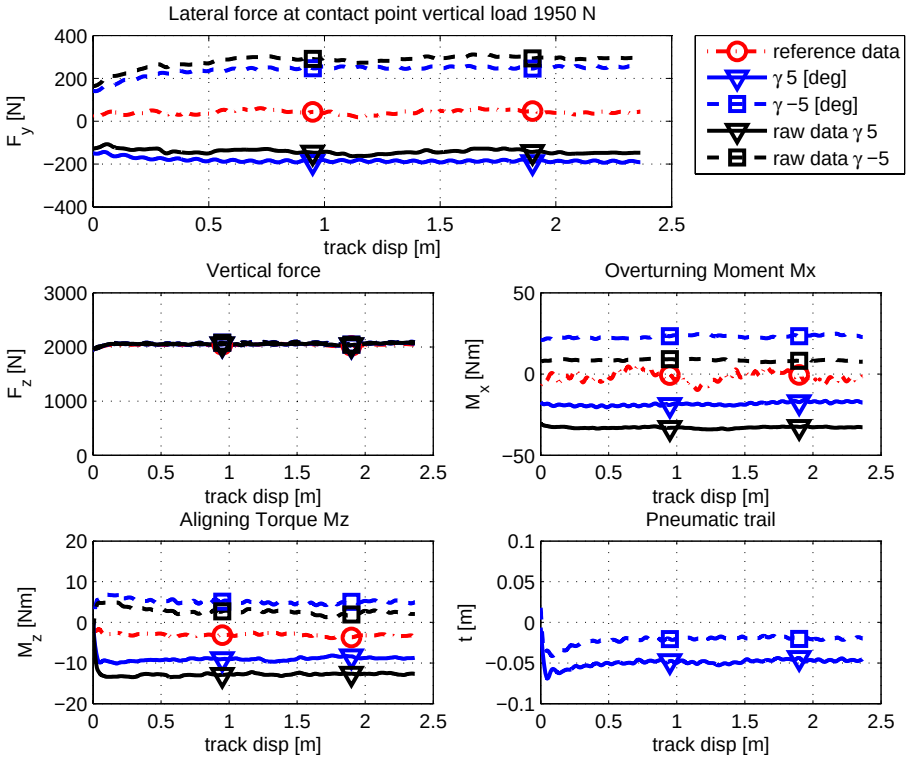

Results measurements old tyre with camber angles of -5 and 5 degrees:
Measurement 37Z:

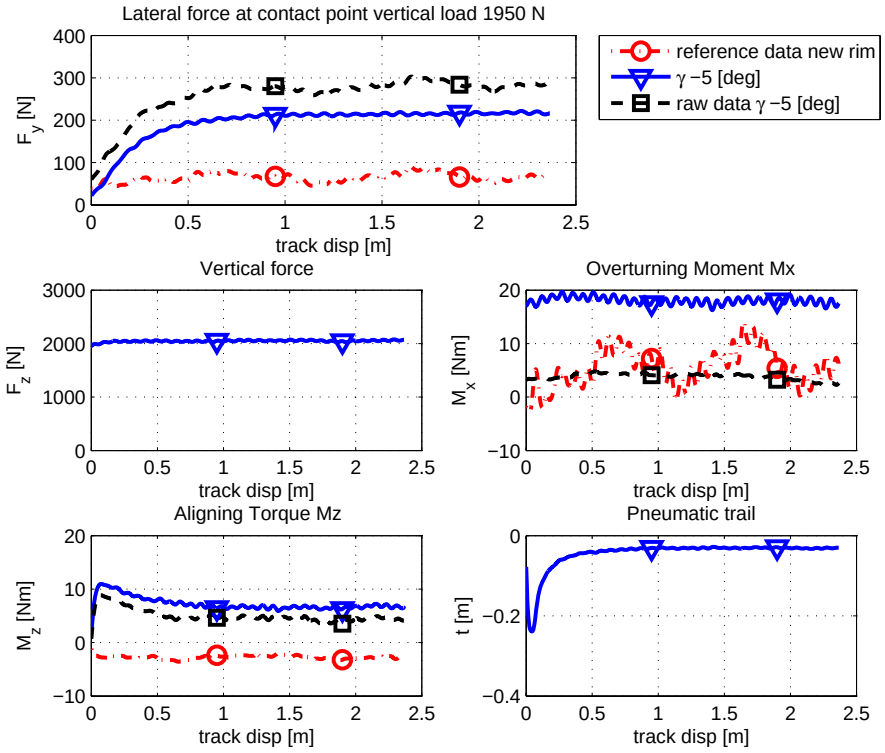

Measurement 38C:

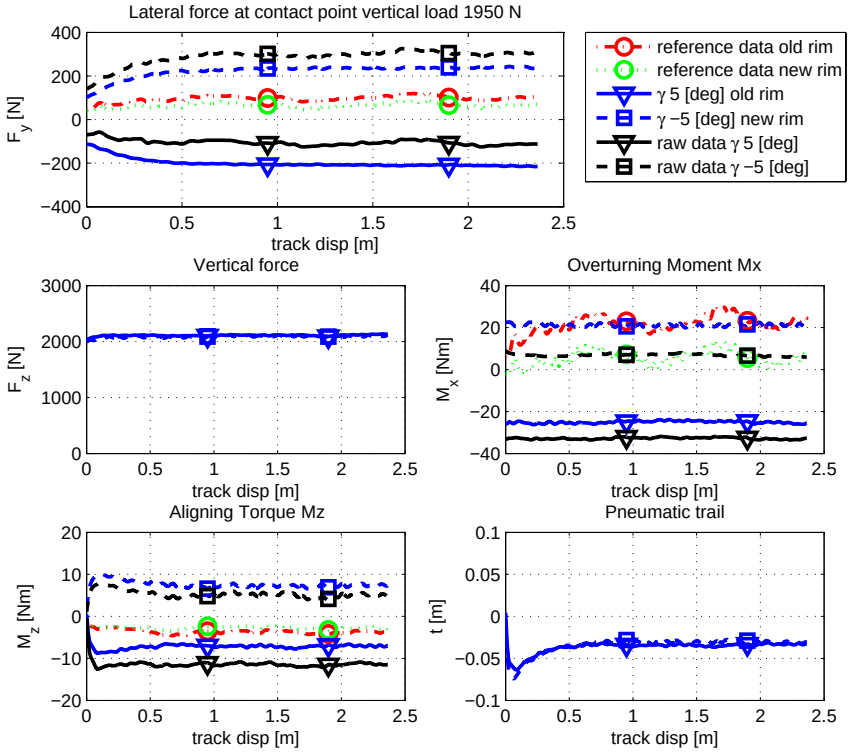

Measurement 38R:

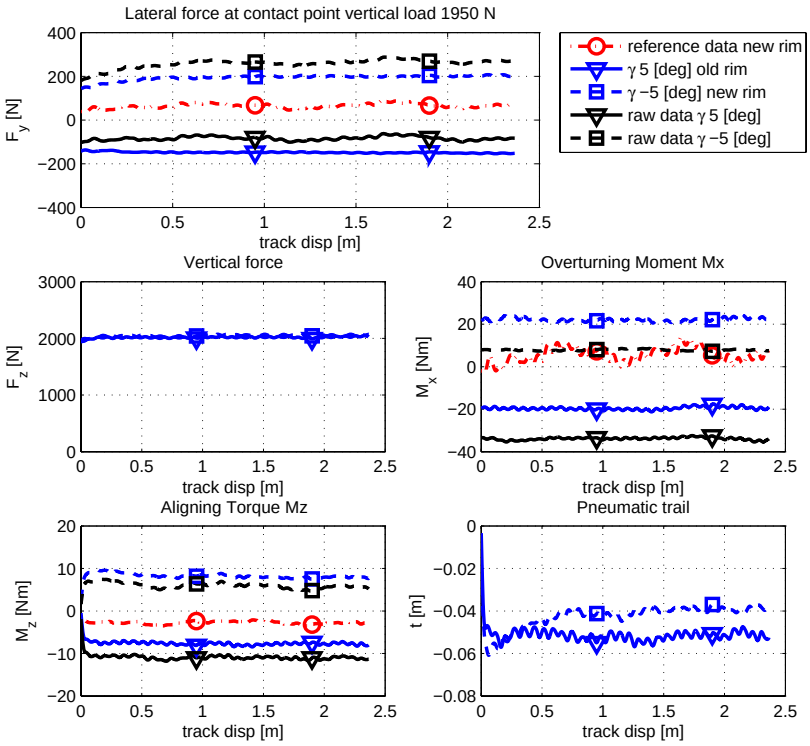

Steady-state results:

Measurement 37Z:

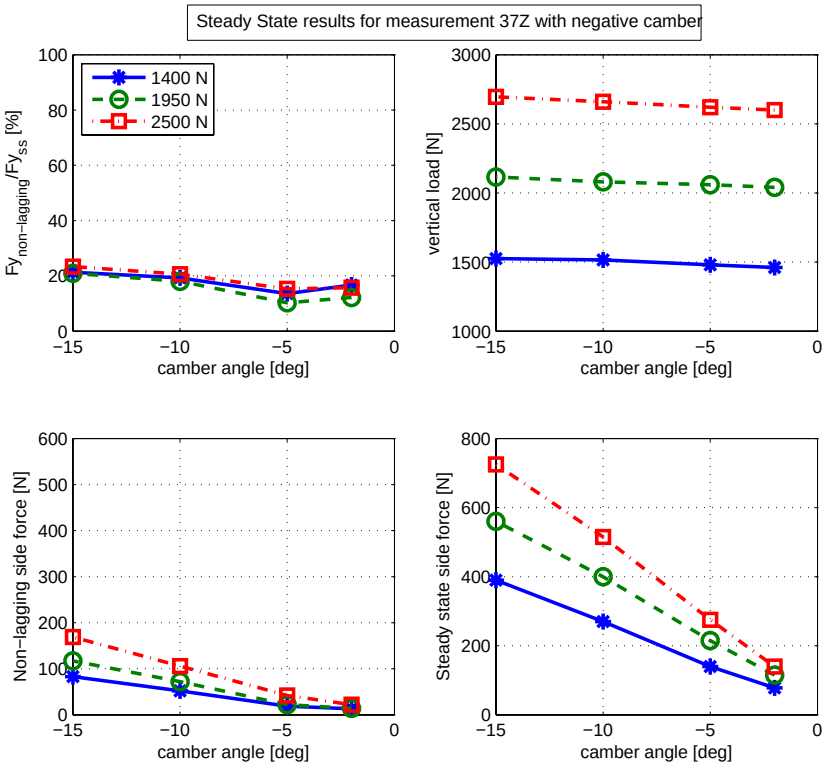

Measurement 38C:

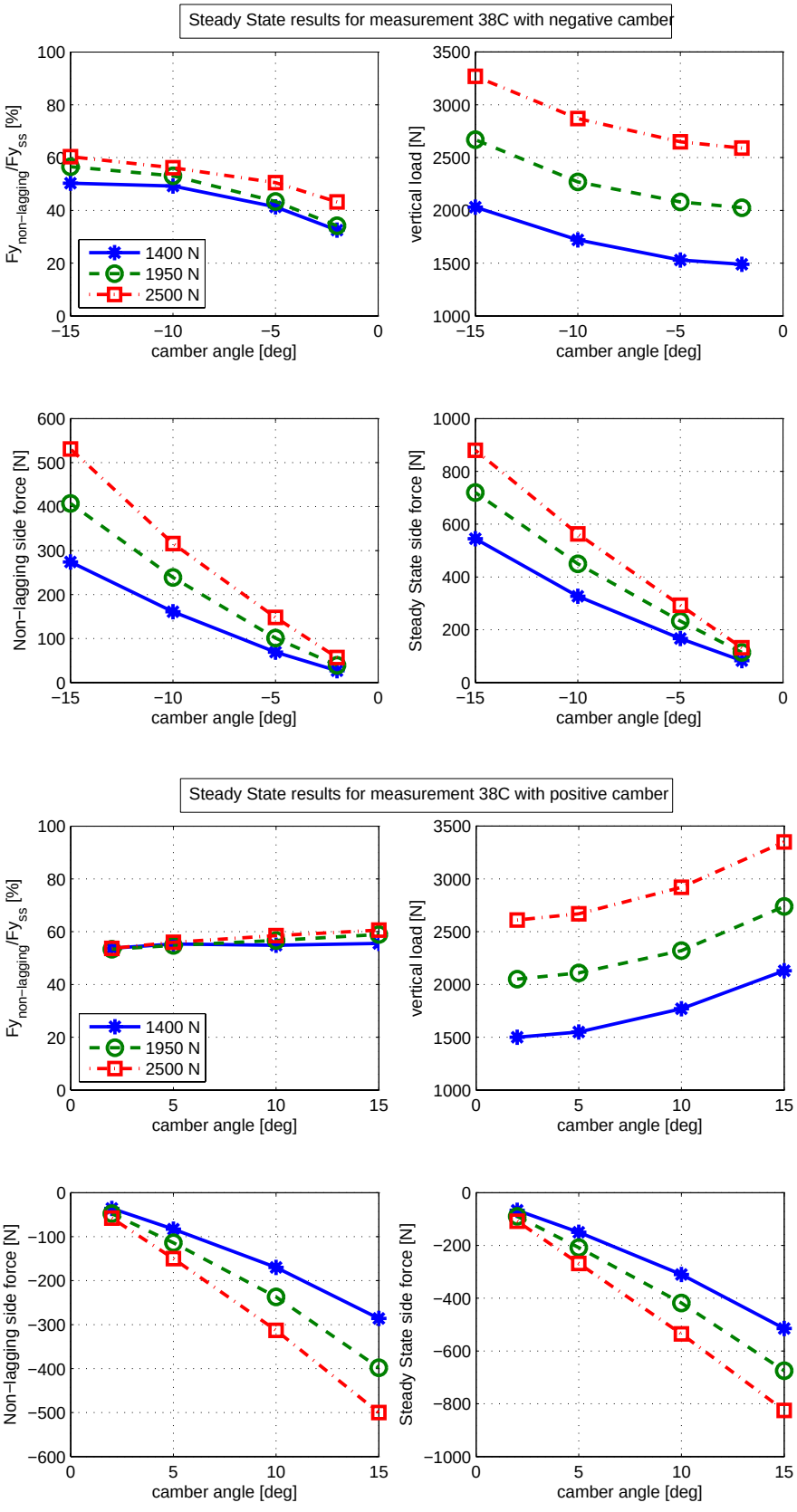

Measurement 38R:

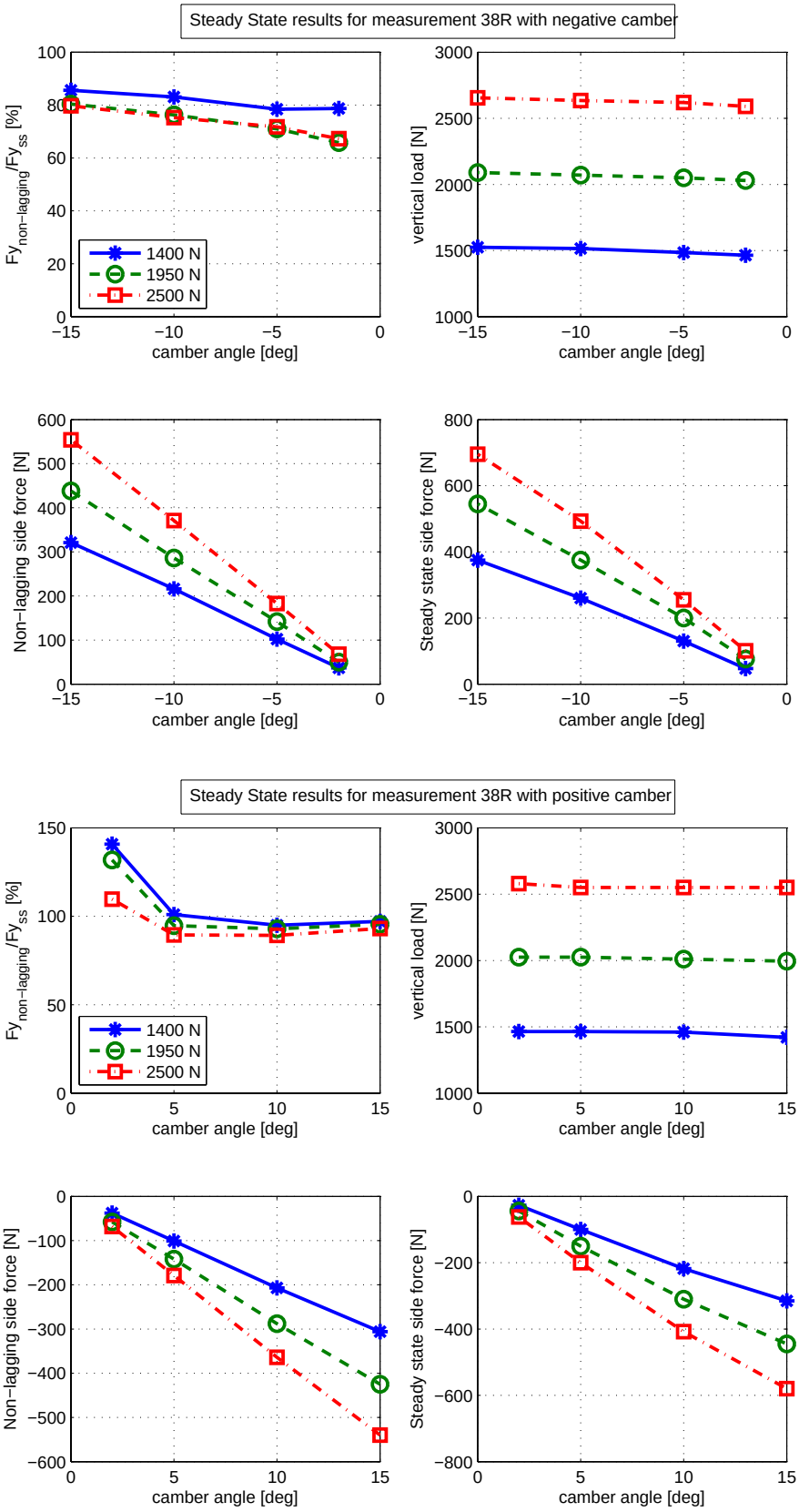

Non-lagging results:

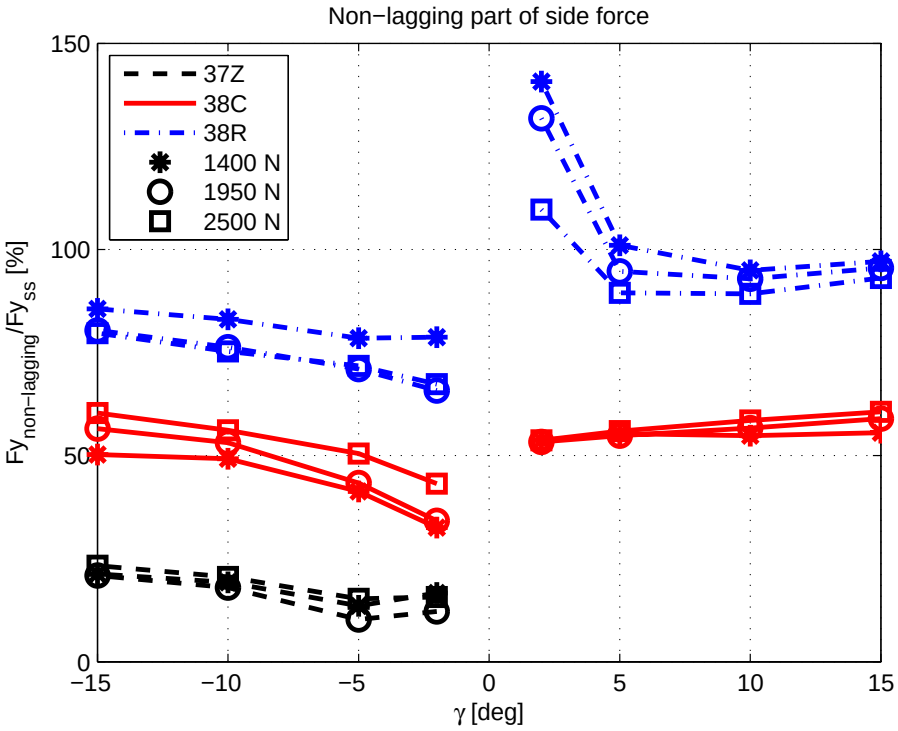

Comparison non-lagging part fraction between old and new tyre: